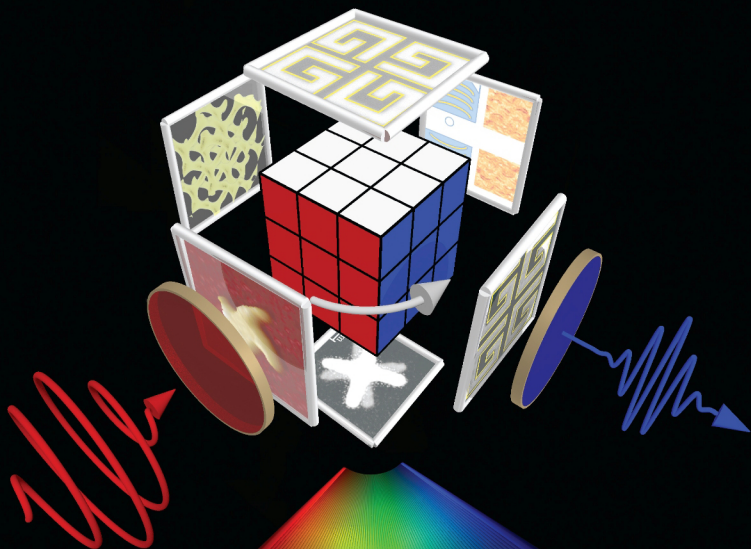


ADVANCED MATERIALS



Chirality and Chiroptical Effects in Plasmonic Nanostructures: Fundamentals, Recent Progress, and Outlook

Ventsislav K. Valev,* Jeremy J. Baumberg, Concita Sibilìa, and Thierry Verbiest

Strong chiroptical effects recently reported result from the interaction of light with chiral plasmonic nanostructures. Such nanostructures can be used to enhance the chiroptical response of chiral molecules and could also significantly increase the enantiomeric excess of direct asymmetric synthesis and catalysis. Moreover, in optical metamaterials, chirality leads to negative refractive index and all the promising applications thereof. In this Progress Report, we highlight four different strategies which have been used to achieve giant chiroptical effects in chiral nanostructures. These strategies consecutively highlight the importance of chirality in the nanostructures (for linear and nonlinear chiroptical effects), in the experimental setup and in the light itself. Because, in the future, manipulating chirality will play an important role, we present two examples of chiral switches. Whereas in the first one, switching the chirality of incoming light causes a reversal of the handedness in the nanostructures, in the second one, switching the handedness of the nanostructures causes a reversal in the chirality of outgoing light.

to coincide with itself".^[1] The word "chirality" derives from the Greek *χειρ* (*kheir*), which means "hand" and, by extension, a chiral object is said to have left or right handedness. Besides hands, living organisms have a large number of chiral constituents. For instance, all the essential amino acids (except glycine) are chiral and all of them have the same handedness. This happens despite the fact that the energy of both chiral forms is equal and their formation has equal probability in an achiral environment. However, only one of the two occurs in nature and the particular handedness involved is the same in humans, animals, plants and microorganisms. Chirality seems to be a basic characteristic of living matter and perhaps even a requirement for life. If one day molecular nanoengineering is to replicate the self-assembling mechanisms of life,

it is likely that chirality will play a crucial role in this future nanotechnology.

As we scale down the dimensions of bulk materials to the nanoscale, unique physical properties are revealed. These properties often arise from the increase in surface-to-volume ratio and from the geometrical confinement of the electrons. A good example can be found in localized surface plasmons (LSP), which are oscillations of free electrons in metals that couple with the electromagnetic field of light.^[2] These LSP can concentrate the electric field at the surface of nanostructures to very small spots - the hotspots - which can then serve as miniature molecular reactors. Within such hotspots, photochemical reactions,^[3] chemical transformations,^[4] and catalytic reactions can take place.^[5,6] These processes are facilitated by the large amplitude of the local electric fields that can give rise to impressive signal enhancements, as in the case of Raman scattering,^[7] which can be increased up to fourteen orders of magnitude.^[8,9] In most cases though, hotspots are highly symmetric and consequently they can be of little use to asymmetric (or chiral) chemical reactions without specifically chiral precursors. Moreover, these hotspots seem to behave essentially as "lenses" for concentrating the field of light. Should the plasmonic nanostructures (10–1000 nm) be chiral, the typical size difference with molecules (< 1 nm) is so large that at first glance it is hard to imagine what could possibly be accomplished with the help of plasmonic nanostructures that cannot be done with

1. Introduction

From small metal clusters of atoms to continuous metal surfaces, and through the whole range of molecular materials, nanomaterials, hybrid materials, bio-materials and metamaterials, chirality splits the material world into left and right and, sometimes, into right and tragically wrong. In his Baltimore lectures on molecular dynamics and the wave theory of light, Lord Kelvin defined chirality as follows: "I call any geometric figure, or group of points, chiral, and say it has chirality if its image in a plane mirror, ideally realized, cannot be brought

Dr. V. K. Valev, Prof. J. J. Baumberg
Cavendish Laboratory
Department of Physics
University of Cambridge
J. J. Thomson Avenue, Cambridge CB3 0HE, UK
E-mail: vkv23@cam.ac.uk

Prof. C. Sibilìa
Dipartimento di Scienze di Base e Applicate per l'Ingegneria
Sapienza Università di Roma
Via A. Scarpa 16, I-00161 Roma, Italy
Prof. T. Verbiest
Molecular Electronics and Photonics
KU Leuven, BE-3001, Belgium



DOI: 10.1002/adma.201205178

sufficiently concentrated light alone. Before considering the importance of plasmonic nanomaterials, let us first consider the classes of chiroptical effects.

Although crucial, chirality is a difficult and subtle property to study scientifically. The reason is that whereas science thrives upon quantifiable information, chirality is essentially a Boolean data type and universal measures have been problematic: an object is either chiral or not. This difficulty can be circumvented because chirality gives rise to several chiroptical effects, which, being quantifiable, serve to informally classify substances as more or less chiral. Chiroptical effects originated from the fact that, in chiral molecules (or *enantiomers*), both the refractive index and the extinction coefficient differ for left- and right-hand circularly polarized light. On the one hand, the difference in refractive index causes *optical rotation*, which is a rotation of the plane of linearly polarized light upon interacting with chiral molecules. On the other, the difference in extinction coefficient causes *circular dichroism*, which is measured as a difference in transmission within chiral molecules, for left and right-hand circularly polarized light. Chiroptical effects are used to determine the enantiomeric excess (or chiral purity) of molecules and the conformation states of biological molecules. More generally, the entire field of chiral photochemistry rests upon the use of chiroptical effects, since these can induce asymmetric synthesis and catalysis.^[10] In all natural materials though, chiroptical effects tend to be very small. As we shall see, plasmonic metal nanostructures not only lead to giant chiroptical effects, but also to some entirely new concepts in physics.

In many organic molecules, chiroptical effects are associated with the tetrahedral bonding structure of carbon that gives rise to chiral centers. At the scale of a few atoms, metal clusters too can be intrinsically chiral.^[11] Moreover, such clusters have malleable electronic properties and even achiral clusters can have chirality bestowed upon them by the presence of chiral surface molecules.^[12] Cluster/molecule chiral nanocomposites are the subject of intense investigation^[13] as the chiroptical effects in them are highly tunable by changing the clusters' size, geometry, spatial arrangement with respect to one another and the nature of the surface molecules.^[14] However metal clusters, typically smaller than $3(\pm 2)$ nm, present discrete energy level in their electronic structure rather than the bands of bulk metal, and consequently they are described as semiconducting and cannot support plasmon resonances. In plasmonic nanostructures, the metal atoms tend to form highly symmetric geometries and, as the size of the nanoparticles increases towards dimensions where the (quasi) bulk metal properties emerge, the optical activity due to intrinsic chirality almost disappears; but not entirely.^[15]

The reason why clusters of metal atoms exhibit chiroptical effects is the symmetry breaking of a few atoms within the crystal lattice. The presence of such asymmetric atoms is not so much related to the size of the nanoparticles as to their crystal lattice. Even continuous metal surfaces can exhibit an abundance of chiral centres; these are the so called kink atoms of high Miller index surfaces, such as Ag(643). In this case, the chirality of the surface arises from single atoms, for instance one at which the (001), (011), and (111) surfaces of a cubic lattice intersect. Moreover, the adsorption of chiral molecules on an achiral continuous metal surface can provoke the



Ventsislav K. Valev is a Research Associate in the Cavendish laboratory at the University of Cambridge. Born in Bulgaria, he grew up in France and graduated in Cardiff, the United Kingdom. In 2006, he was awarded a Ph.D. from the Radboud University of Nijmegen in the Netherlands, and subsequently, became a postdoc-

toral fellow at the KU Leuven University in Belgium, where he worked on second harmonic generation from chiral organic molecular films and chiral nanostructured metal surfaces.

local relaxation of metal surface atoms causing the surface to become chiral. This is known as chiral footprinting, and has been reported from (R,R)-tartaric acid on Ni(110),^[16] or (R,R)-bitartrate on Cu(110).^[17] Therefore, nanopatterning continuous chiral metal surfaces could in principle result in chiral plasmonic nanoparticles. Moreover, just as with clusters, chirality can be achieved in plasmonic nanoparticles by changing their geometry, their spatial arrangement with respect to one another and the nature of surface molecules. However not only the chiral geometry of these nanoparticles is of interest, but also their chiroptical behavior, where plasmons are used to manipulate the local electric and magnetic fields.

Assemblies of chiral plasmonic nanoparticles exhibit strong electric, magnetic and Fano-type resonances.^[18] The characterization of these resonances involves near-field electromagnetic coupling of dipoles and multipoles, as well as long-range radiating mechanisms, such as antenna effects. Because of the strong interplay between local electric and magnetic fields, these mechanisms significantly enhance the chiroptical effects. Strong chiroptical effects have thus been reported from plasmonic nanoparticles assembled on the chiral scaffolds of organic fibers,^[19] or in nanoparticles that are assembled in chiral superstructures.^[20,21] Such structures can also be elegantly assembled with the help of molecules, like DNA,^[22] and conversely, the plasmonic nanoparticles can enhance the chiroptical response of nearby chiral molecules.^[23–25] Even achiral nanoparticles have been shown to exhibit strong chiroptical responses due to a long-range coupling through a layer of chiral molecules.^[26] In fact, the chirality of plasmonic nanostructures plays a fundamental role in an entire new class of materials–metamaterials.

Metamaterials have recently emerged as one of the most prominent topics of material research. Metamaterials are materials artificially engineered to possess unusual electromagnetic properties.^[27–29] These materials can be constructed from periodic arrays, with a unit cell usually much smaller than the wavelength of light. Consequently, whereas natural materials derive their properties from those of their constituent atoms and molecules, artificial metamaterials derive their properties

from those of their nanoengineered unit cells. A key aspect of metamaterials is the achievement of negative refractive index.^[30] To this purpose, both the electric permittivity ϵ and the magnetic permeability μ of the material must be negative over the same spectral range. An important challenge for metamaterials has therefore been to nanoengineer unit cells that can satisfy the restrictive requirements for negative refractive index, for instance by making use of split-ring resonators. Recently an alternative route towards negative refractive index has been discovered, that makes use of chirality.^[31–33]

Chiral metamaterials with negative index of refraction have been assembled for the microwave regime,^[34–36] the terahertz,^[37] and for optical frequencies.^[38,39] Efforts in designing such metamaterials have progressed towards increasing the linear^[40] and nonlinear^[41] chiroptical behaviour, combining chirality with split-ring resonators through twisting them,^[42,43] moving away from planar nanostructures towards more pronounced three-dimensional configurations,^[44] and towards more isotropic materials.^[45] In addition to the benefits of negative refractive index, chiral metamaterials recently attracted much interest because of their strong optical rotation, potential for slow light applications and the possibility for use as broadband circular polarizers.^[46] Moreover, chiral metamaterials constitute a candidate for achieving *repulsive* Casimir forces, which could lead to frictionless nanomotors, based on nanolevitation.^[47] For a recent review on chiral metamaterials, see Ref. ^[48]. Perhaps even more important is the fact that metamaterials can be used to enhance the optical response of chiral molecules even further by a novel method—through use of superchiral light.

The reason why chiroptical effects are small in molecules resides in the fact that the chiral arrangement of molecular bonds occurs over a much smaller distance than the helical pitch of circularly polarized light. One way to increase the chiroptical effects consists therefore of increasing the chiral pitch of the material to match that of circularly polarized light. This has been demonstrated with cholesterical liquid crystals, where circularly polarized light with the same handedness as that of the liquid crystal is almost perfectly reflected.^[49] Another way is to compress the helical pitch of circularly polarized light to the scale of the material. Such “superchiral” light has been achieved in free space by making use of stationary, counter propagating waves to realize a field with very strong twist near the nodes, which indeed resulted in an enhanced optical response from chiral molecules.^[50] Furthermore, it was shown that the creation at discrete points in space of all valid configurations of electric and magnetic fields and field gradients is possible but would require the superposition of up to 32 linearly polarized monochromatic plane waves;^[51] which obviously is not very practical. It is therefore interesting to consider the fields with complex spatial profile that can be generated by plasmonic metamaterials.^[52] Such materials could then be successfully used to enhance the enantioselectivity at surfaces,^[50] which holds great potential for chiral photochemistry.

It is clear that chiral plasmonic nanoparticles and nanomaterials are poised for playing a key role in technological developments, however, we believe that it is also appropriate to mention the dangers that chirality has already tragically revealed for molecular materials.

While writing this manuscript, a bronze memorial was inaugurated in the city of Stolberg (Germany) on August 31, 2012 to commemorate the victims of the thalidomide tragedy. Over fifty years ago, thalidomide was released as painkiller medication and administered to thousands of pregnant women in the world against morning sickness. The drug has a chiral structure, but being synthesized in an achiral environment, both enantiomers were produced and both were administered. Although the mirror image of some chiral drugs is harmless, for others it is an “evil twin” and unfortunately this is the case with thalidomide. In pregnant women, the drug’s “evil twin” fixed itself to the DNA of the growing fetus and inhibited the expression of genes that control the development of limbs. As a consequence, over ten thousand babies worldwide were born without limbs or with shortened limbs.

Thalidomide is far from being the only chiral molecule that has an “evil twin”. Other examples include an enantiomer of ethambutol fighting tuberculosis, whose “evil twin” causes blindness, one enantiomer of naproxen reducing arthritic inflammation while its “evil twin” poisons the liver and methamphetamine, used as a non-prescription over-the-counter nasal decongestant, with its “evil twin” being the well-known psychostimulant crystal meth.^[53] As the consequences of releasing thalidomide became clear, chirality became highly important for the pharmaceutical and drug industries. The tragedy highlighted the need for *optically pure* (i.e., containing a single enantiomer) molecular compounds and methods for precisely measuring chirality. This need for highly sensitive chiroptical effects certainly extends to chiral plasmonic nanostructures as well, whose effect upon release in the environment is still largely unknown.

As chiral plasmonic nanostructures are mainly being developed for their optical properties, experimental methods that are highly sensitive to chiroptical effects are of prime concern. In the following, we shall start by presenting chiral plasmonic nanostructures in more detail. To this purpose, the assembling strategies, the production methods and the concept of localized surface plasmons will be briefly described. Next, we shall introduce the main linear chiroptical effects, namely optical rotation (OR) and circular dichroism (CD), as well as their nonlinear optical counterparts in second harmonic generation (SHG), i.e., SHG-OR and SHG-CD. Further on, we shall present four cases where plasmonic nanoparticles have been demonstrated to lead to very strong chiroptical effects. These cases consecutively highlight the importance of chirality in the nanostructures themselves (for linear and nonlinear chiroptical effects), in the experimental setup and in the light itself. Finally, we shall give an outlook towards future developments where the manipulation of chirality will play an important role. In particular, we will focus on chirality switches and give two examples: one where reversing the chirality of incoming light can be used to switch the handedness of the nanostructures and one where reversing the handedness of the nanostructures switches the chirality of outgoing light. Please note that this Progress Report is not intended as a comprehensive review of the subject, but rather as a selection of helpful insights chosen from the recent literature and from our direct experience of the subject.

2. Chiral Plasmonic Nanostructures

2.1. Chirality from Molecules to Nanostructures

The nanoengineering strategies that have been developed for chiral nanostructures can be related to concepts that originated in chiral molecules. **Figure 1** summarizes these concepts, namely: helical chirality, chiral coupling, supramolecular chirality, pseudo or extrinsic chirality and assembly upon chiral scaffolds.

Helical chirality is exhibited by both propeller and spiral types of structures. For example, Figure 1a shows the perchlorotriphenylamine molecule, whose overall aspect evokes the shape of a three-arm helix. Similarly, nanostructures that consist of helices with four rectangular arms have been prepared and were found to exhibit giant optical activity, see Figure 1b. More recently, helices with four curved arms, in Figure 1c, were shown to exhibit strong nonlinear circular dichroism. As an example of spiral chirality, the helicenebisquinone molecule is displayed in Figure 1d. Because this molecule is conjugated

over its spiral length, electrons can move along and give rise to large nonlinear chiroptical effects. In an attempt to emulate this behavior, the 2D spiral nanostructure in Figure 1e, was conceived. Later, a nanomaterial consisting of 3D spirals was constructed and demonstrated to act as a broadband circular polarizer. An alternative way to achieving chirality is to couple achiral elements, such as the two building elements of the 2,2'-dimethoxy-binaphthyl molecule, in Figure 1g. Similar coupling mechanisms were explored for nanostructures with crosses, in Figure 1h, which were shown to exhibit strong chiroptical behavior, both at the fundamental wavelength and at the second harmonic. Moreover, very interesting effects were achieved upon superimposing two resonant U-shaped nanostructures and varying their mutual orientation, see Figure 1i. The coupling of these split-ring resonators was used to introduce the concept of stereometamaterials, directly inspired from stereochemistry.

Another well known concept in chemistry is supramolecular chirality, represented in Figure 1j. In this case too, chirality is achieved through coupling however, because the building

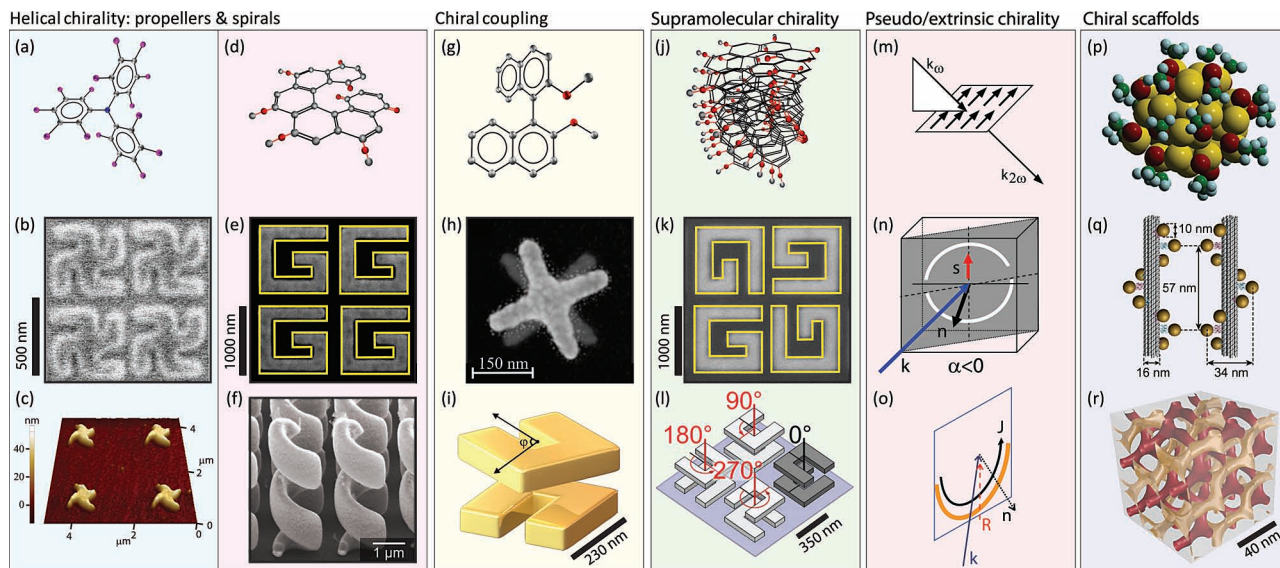


Figure 1. Many of the concepts associated with chirality that have initially been developed for molecules are nowadays being transferred to nanostructures. In (a), the perchlorotriphenylamine molecule has the shape of a propeller, which is an example of helical chirality. Correspondingly, propeller-shaped nanostructures, in (b)^[54] and (c),^[55] also exhibit this form of chirality. Another example of helical chirality is found in spiral-shaped molecules, such as the helicenebisquinone, in (d). Analogously, 2D and 3D spirals can be constructed from nanostructures, in (e)^[56] and (f)^[46] respectively. Chirality is also achieved upon coupling two or more achiral molecules, as illustrated by the 2,2'-dimethoxy-binaphthyl molecule, in (g). Similarly the superposition of achiral crosses, in (h)^[57,58] and split-rings, in (i),^[59] results in chiral nanomaterials. The chiral coupling of molecules that are themselves chiral results in supramolecular chirality; in (j) the spiral is formed by stacking such molecules as the one in (d). For nanostructures, the concept of supramolecular chirality can find applications in both 2D and 3D, in (k)^[56] and (l)^[60] respectively. Pseudochirality is an effect whereby tilting of the plane containing anisotropic molecules can result in optical activity, without the presence of actual chiral species, as schematized in (m).^[61] The idea has also been successfully transferred to nanostructures in the case of both the linear^[62] and nonlinear optics,^[63] in (n) and (o) respectively. Moreover, chirality can arise from the interactions of molecules and nanostructures; typically one attaches these to a chiral scaffold. Such hybrid chiral materials can be as small as clusters, in (p),^[64] or as large as DNA molecules and metamaterials, in (q),^[65] and (r) respectively. Panel (b) adapted with permission from Ref. 54. Copyright 2005, American Physical Society. Panel (c) adapted with permission from Ref. 55. Copyright 2012, American Optical Society. Panel (e) adapted with permission from Ref. 56. Copyright 2009, American Chemical Society. Panel (f) adapted with permission from Ref. 46. Copyright 2009, American Association for the Advancement of Science. Panel (g) adapted with permission from Ref. 57. Copyright 2011, American Optical Society. Panel (h) adapted with permission from Ref. 58. Copyright 2009, Nature Publishing Group. Panel (i) adapted with permission from Ref. 59. Copyright 2010, American Optical Society. Panel (m) adapted with permission from Ref. 61. Copyright 1996, American Physical Society. Panel (n) adapted with permission from Ref. 62. Copyright 2009, American Physical Society. Panel (o) adapted with permission from Ref. 63. Copyright 2011, American Physical Society. Panel (p) adapted with permission from Ref. 64. Copyright 2009, Royal Society of Chemistry. Panels (q,r) adapted with permission from Ref. 65. Copyright 2012, Nature Publishing Group.

blocks are themselves chiral, the optical activity can be additionally reinforced. Transposing this concept to nanostructures, the pattern in Figure 1k shows four 2D spirals (or G-shaped nanostructures), that have been themselves arranged in a chiral fashion. The arrangement gives rise to strong nonlinear circular dichroism that was attributed to chiral coupling of the nanostructures. In Figure 1l, four U-shaped nanostructures have been arranged in a chiral pattern and then, on a second layer, the same chiral pattern is repeated and rotated 90°, thereby effectively mimicking 3D supramolecular chirality. Chiroptical effects can be measured even from achiral molecules, provided that they are anisotropic and are illuminated at an angle of incidence different than zero. In such a configuration, the experimental geometry is chiral. This phenomenon is referred to as *pseudo* or *extrinsic* chirality and, for instance, it was demonstrated in the nonlinear optical regime for 2-docosylamino-5-nitropyridine molecules and is schematically represented in Figure 1m. Similar schematic representations were used to indicate the extrinsic chirality that was observed in nanostructures in both the linear (Figure 1m) and the nonlinear (Figure 1o) optical regimes. Moreover chiral nanostructures are literally building upon the knowledge of chiral molecules whenever chiral scaffolds are involved in the construction of chiral nanomaterials. In Figure 1p, chiral molecules that bind onto the scaffold of a chiral gold cluster enhance the optical activity of that cluster. Conversely, in Figure 1q, gold nanoparticles binding to a strand of DNA follow the chiral arrangement of the molecule. Of special interest for self-assembling large scale 3D chiral metamaterials are chiral block copolymers, which can be used to prepare nanostructures with gyroid geometry such as the one shown in Figure 1r.

2.2. Bottom-Up and Top-Down Preparation of the Nanostructures

Nanomaterials are generally prepared following bottom-up and top-down approaches. In the former case, typical methods are colloidal self-assembly and electrochemical deposition of metals upon chiral self-assembled molecular networks. Top-down techniques include focused ion beam lithography, electron beam lithography and direct laser writing.^[66] These general methods can also be applied to the preparation of chiral nanostructures, where they exhibit the same advantages and limitations.

On the one hand, self-assembly is largely regarded as holding the keys to real world applications of nanotechnology, as it is cheaper, faster, can be employed to produce industrial quantities of nanoparticles and, quite importantly, it can be regarded as our best chance to reverse-engineer and implement the self-assembling principles of life. On the other, self-assembled nanomaterials struggle to produce monodispersed nanoparticles, are limited mainly to simple geometries such as spheres or rods and struggle to maintain order over large distances. The situation is almost entirely reversed in the case of top-down approaches, which offer excellent design flexibility, yet they are also costly, time-consuming, and can hardly be considered for industrial scale production, let alone artificial life. As a consequence, both approaches to nanotechnology assembly can be viewed as complementary; top-down methods being used to

unravel the principles upon which self-assembled future nanotechnology will grow. Chiral nanostructures are subject to the same general trends, though, in addition, they often require rather complex geometries. Figure 2 shows two examples of such complex nanogeometries being achieved through bottom-up and through top-down methods.

In Figure 2a, an isoprene-*block*-styrene-*block*-ethylene oxide (ISO) block copolymer (BCP) is shown that forms two chemically distinct, interpenetrating gyroid networks (blue and red) of opposite chirality in a third block matrix, which is shown in gray.^[69] This type of structure is particularly interesting because the two chiral networks have distinct chemical properties and can be separately dissolved. In Figure 2b, the isoprene block is thus removed and the space it leaves can be back-filled with gold through electrodeposition, see Figure 2c. The gold gyroid constitutes a self-supporting material network that can be uncovered upon plasma etching of the two remaining polymer blocks, see Figure 2d.

Polymer layers are also employed in the top-down technique of electron beam lithography (EBL). Figure 2e shows electron beam patterning of a G-shaped nanomaterial design on polymethyl methacrylate (PMMA). Once the design pattern is completed, the irradiated area is dissolved and the remaining area is baked resulting in the EBL mask, in Figure 2f. Next, gold is deposited through sputtering in a high vacuum chamber (Figure 2e). The gold is deposited within the designed area as well as on top of the remaining polymer. The latter can then be removed through immersion in a solvent, such as warm acetone or dichloromethane, for a few minutes. Following the last step of the preparation procedure, only the chiral gold nanostructures are left on the substrate and their plasmonic properties can be investigated.

2.3. Localized Surface Plasmon Resonances

Localized surface plasmon resonances (LSPR) are typically observed in metal nanoparticles, often made of Au or Ag, with dimensions significantly smaller than the wavelength of light. Within the small dimensions of such particles, light can effectively be confined, which results in local electromagnetic field enhancements. In coinage metals, the enhancements are related to electrons in the conduction band, whose energy matches that of visible light. As a result, light causes the surface electrons to oscillate coherently and, depending on the size of the nanostructures, their constitution, their geometry, their surroundings and their distance from each other, a strong resonance can be achieved for a given wavelength of light. At resonance, strong absorption and scattering of the light can be observed from nanoparticles. In Mie's theory, for a spherical nanoparticle with radius (R) such as $R/\lambda \ll 1$ (where λ is the wavelength of light), this light-matter interaction is characterized by the extinction coefficient:

$$C_{ext} = \frac{24\pi^2 R^3 \epsilon_m^{3/2} N}{\lambda \ln(10)} \frac{\epsilon_i}{(\epsilon_r + 2\epsilon_m)^2 + \epsilon_i^2} \quad (1)$$

where N is the electron density, ϵ_m is the dielectric constant of the surrounding medium and $\epsilon = \epsilon_r + i\epsilon_i$ is the complex

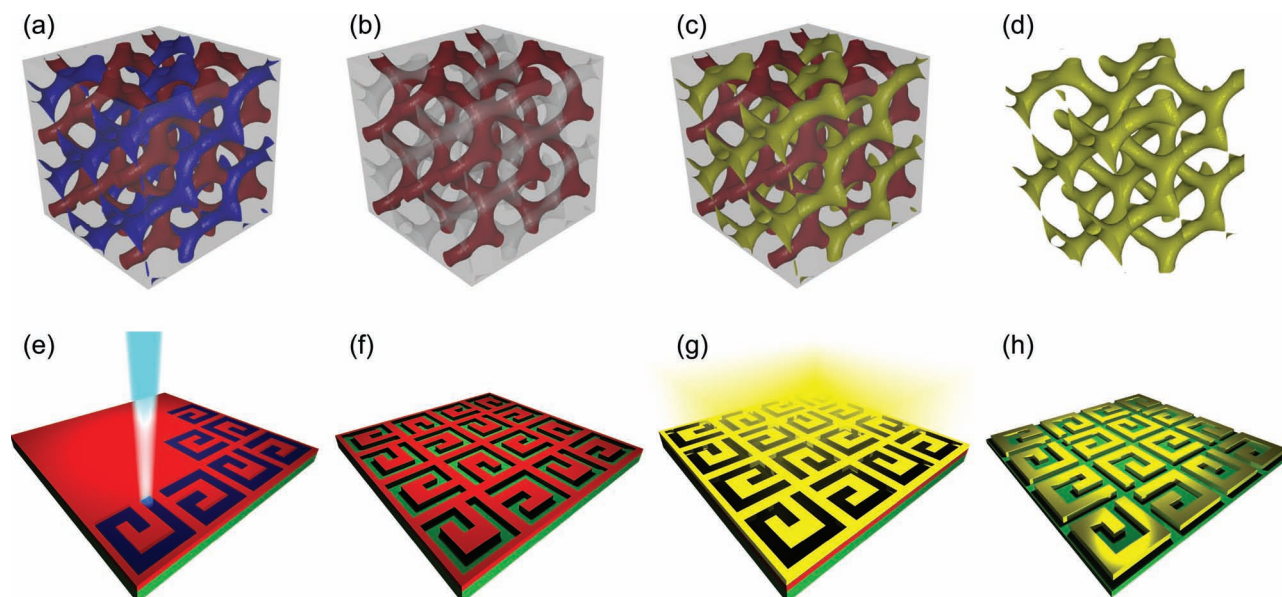


Figure 2. Examples of bottom-up and top-down preparation of chiral nanostructures. In the first case, the material preparation proceeds from the self-assembly of a block copolymer.^[67] In (a), the three different colors (red, blue, and grey) correspond to the different blocks of the copolymer. The isoprene block (blue) is removed in (b) and is then back-filled with gold (yellow) in (c). The final structure is obtained by plasma etching the two remaining polymer blocks, revealing a 3D continuous gold network in air, in (d). In the case of top-down material preparation, the nanostructure pattern is drawn on a resist layer with electron beam lithography, in (e).^[68] Subsequently, the resist within the pattern is removed with a solvent bath, producing a mask, which is shown in (f). The mask is then subjected to metal evaporation, in (g). Next, upon lift-off, all the resist is removed with a second solvent bath producing (h). Panels (a–d) adapted with permission from Ref. 67. Copyright 2012, Wiley. Panels (e–h) adapted with permission from Ref. 68. Copyright 2011, American Optical Society.

dielectric constant of the bulk metal. It follows that, for a spherical nanoparticle, the resonance is achieved when $\epsilon_r = -2\epsilon_m$

An intuitively very appealing way to look at this resonance is to consider that the electron cloud of the nanoparticle can be modeled as a harmonic oscillator. The cloud can then be viewed as subjected both to the force exerted on the charges by the electric field of light and to the restoring force of the positively charged metal cores. In response to these forces, the electron cloud oscillates at the frequency of light, see **Figure 3a**. The distortion of the electron cloud in response to the electric field of light can be expressed as the polarisability:

$$\alpha(\lambda) = 4\pi\epsilon_m(\lambda)R^3 \frac{\epsilon(\lambda) - \epsilon_m(\lambda)}{\epsilon_m(\lambda) + 2\epsilon_m(\lambda)} \quad (2)$$

where the maximum polarization corresponds to the resonance condition in the denominator. An increase in the dielectric constant of the surrounding medium leads to an increased electric field within the dielectric, which opposes the local electric field at the surface of the nanoparticle and reduces the restoring force. Consequently the resonance frequency of the oscillator drops, so the plasmon resonance red-shifts. A red-shift can also be observed upon varying the shape of the nanoparticle. For non-spherical nanoparticles, the resonant condition takes the form $\epsilon_r = -\chi\epsilon_m$, where χ is the shape factor, which is equal to 2 in the case of a sphere and increases with the aspect ratio. In the case of chiral geometry, the situation becomes significantly more complex.

To tackle chiroptical effects, Mie's theory has been extended by Bohren to account for circular dichroism and optical rotation in an optically active sphere.^[70] More recently, simulations have been performed in order to compare the optical activity of a sphere with actual experimental results, whereby a scattering solid angle towards the aperture of a detector was taken into account.^[71] These calculations however focus on very small nanoparticles, whereas the chiral nanostructures in **Figure 1** range from 50 nm to the micron scale. At this scale, retardation effects play an important role. Moreover, **Figure 1** reveals that chiral geometries exhibit kinks and sharp corners, where the geometric confinement of the fields, known as the electrostatic lighting rod effect, needs to be taken into account. Because of the increase in complexity, the electromagnetic properties of chiral nanostructures are simulated numerically, by means of Maxwell equations' solvers, such as MAGMAS,^[72,73] Lumerical,^[74] MEEP,^[75] RSoft's DiffractMOD,^[76] etc. Nevertheless, some degree of intuitive understanding can be achieved by considering that upon interacting with a spherical nanoparticle, circularly polarized light drives the electron cloud in a spiral, see **Figure 3b**. This case of polarization gives rise to an electric current on the surface of the nanostructure as the charges are pushed away from the propagating electric field of light. Therefore, for a given direction of circularly polarized light, the chiral geometry of a metal nanostructure can either accommodate the surface current or hinder it, see **Figure 1c** and **1d**. It should be noticed though that this intuitive picture does not take into account the finite dimensions of the chiral path. In reality, the

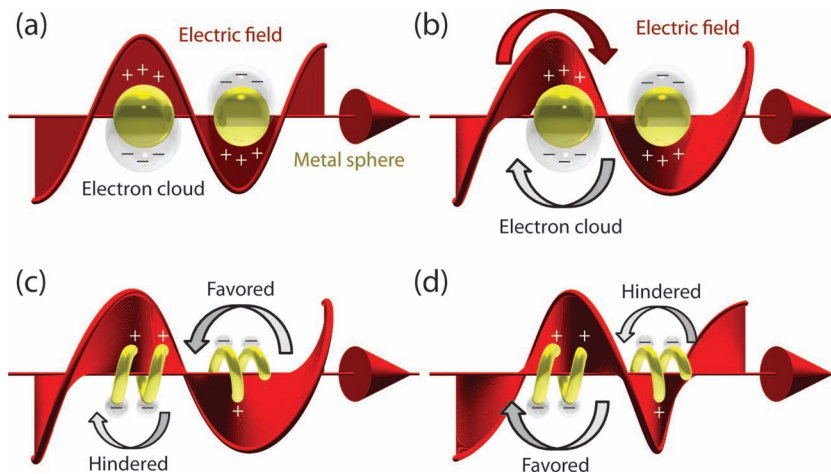


Figure 3. The interactions between chiral nanoparticles and circularly polarized light can be understood intuitively. In (a), a schematic diagram illustrates how the oscillating electric field of linearly polarized light can drive the oscillation of the electron cloud in a metal nanoparticle. In (b), the rotating electric field of circularly polarized light causes the electron cloud to rotate around the nanoparticle. In the case of chiral nanoparticles, the rotation of the electron cloud under illumination with circularly polarized light can be favored or hindered depending on the combination of chiral geometry and direction of circularly polarized light, as it is shown in (c) and (d).

spiral could form a cavity for circularly polarized light, whereby currents are reflected back from the edges, accommodating different eigenmodes at different wavelengths, as was shown in Ref. 46. In the next section, we shall briefly cover some of the main chiroptical effects in linear optics and see that they are very different from their nonlinear counterparts.

3. Chiroptical Effects

Whereas the linear chiroptical effects of optical rotation (OR) and circular dichroism (CD) can be understood in a very straightforward and intuitive way, their nonlinear counterparts in second harmonic generation (SHG-OR and SHG-CD) are significantly less obvious. Moreover, whereas the linear chiroptical effects require that both electric and magnetic dipoles be taken into account, the nonlinear ones can exist for electric dipoles alone. As a consequence, linear and nonlinear chiroptical effects are sensitive to different aspects of chirality.

3.1. Linear Chiroptical Effects

Upon encountering a material medium, light propagating is controlled by its refractive index n and its extinction coefficient k . The extinction coefficient corresponds to a measure of how much a substance scatters and absorbs electromagnetic radiation and

this coefficient affects the amplitude of the emerging electric field of light. As for the refractive index, it indicates the reduction of the speed of light in the material. Depending on the particular material, light can interact either dominantly with n or k , or equally with both. Linearly polarized light, which is represented with a blue arrow in Figure 4a, can be considered as a combination of left- (σ^-) and right-hand (σ^+) circularly

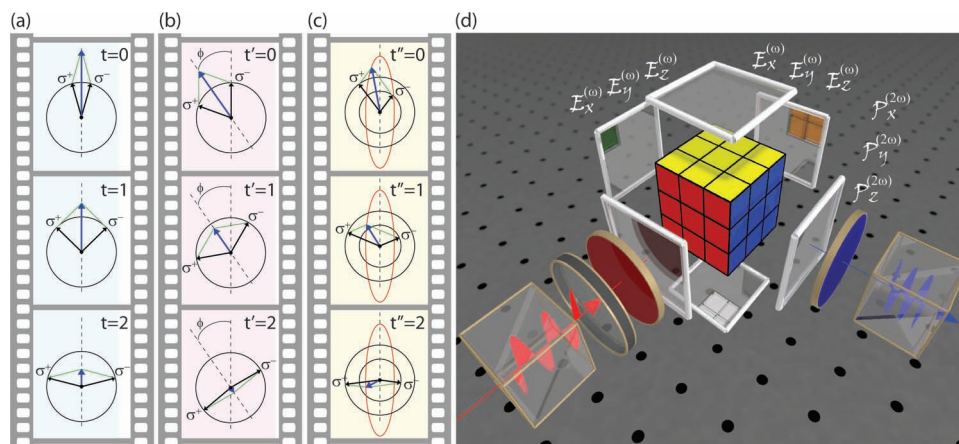


Figure 4. Whereas the physical mechanism of optical activity is very straightforward in linear optics, in second harmonic generation it is not. Linearly polarized light (blue arrow) can be considered as a combination of left- and right-hand circularly polarized waves, represented in (a) by the two black arrows σ^+ and σ^- , at times $t = 0$, $t = 1$, and $t = 2$. In (b), due to the interactions with a chiral material, left and right-hand circularly polarized waves can propagate with same amplitude but different phase velocities. In this case, σ^+ and σ^- have the same amplitude, though, at time $t' = 0$, σ^+ has not completed its circular evolution. Subsequently, at times $t' = 1$ and $t' = 2$, the resulting linear polarization vector appears to be rotated from its original position by an angle ϕ —the angle of optical rotation. In (c), due to the interactions with a chiral material, left- and right-hand circularly polarized waves can propagate with same phase velocities but different amplitude. In this case, σ^+ and σ^- have completed the same circular evolution, though, at time $t'' = 0$, σ^- is shorter. Subsequently, at times $t'' = 1$ and $t'' = 2$, the resulting field polarization vector follows an elliptical path. In (d), second harmonic generation originates from the nonlinear susceptibility tensor. This tensor is composed of $3 \times 3 \times 3$ components, which can be represented by a cube with side 3. The presence of chirality within the material results in the appearance of characteristic tensor components, which directly affect the polarization state of the second harmonic radiation.

polarized light. At time $t = 0$ and subsequently, these circularly polarized light waves have equal amplitudes and angular velocities, as indicated by the black arrows. For chiral materials, both the refractive index and the absorption coefficient of one material handedness differ for left- and right-hand circularly polarized light.^[10]

First, we shall consider the case where left- and right-hand circularly polarized light propagate within a medium with different phase velocities, due to chirality. Upon emerging from the medium, the arrows σ^- and σ^+ would have completed different parts of their circular evolution. Since there is no difference in absorption, both arrows possess equal amplitudes. The resulting polarization is schematized in Figure 4b, where, at time $t' = 0$, σ^- has not completed its circular evolution and the resulting net linear polarization vector (blue arrow) is rotated from its original position by an angle ϕ . This effect is called *optical rotation* or *circular birefringence*. When conducted as a function of wavelength, this is called *optical rotatory dispersion* (ORD). The angle of optical rotation is expressed as $\phi = \pi(n^+ - n^-)l/\lambda$, where n^+ and n^- indicate the refractive index for left- and right-hand circularly polarized light, λ is the wavelength and l is the path length within the material. For chiral molecular materials, the difference in refractive index is typically around 10^{-6} but with sufficient path length, several degrees rotation can be measured. Optical rotation is intrinsically linked with the spatial variation of the electric field on the length scale of the molecule or nanostructure.

Next, we consider the situation where, due to the presence of chirality, left- and right-hand circularly polarized light are affected differently by the extinction coefficient. In this case, σ^- and σ^+ would have the same phase velocity upon emerging from the chiral material and they would have completed the same circular paths. Consequently, there would be no rotation of the linear polarization vector ($\phi = 0$). However, since the two circular polarizations do not experience the same amount of scattering and absorption in the chiral material, the relative amplitude of their vectors would have changed. In Figure 4c, it is shown that, at time $t'' = 0$, the arrow σ^- has a smaller amplitude than σ^+ and has completed a smaller circle. Subsequently, the resulting field polarization follows an ellipse, and hence it is said to exhibit *ellipticity* denoted by ϵ . Quantitatively, the ellipticity is defined as $\tan \epsilon = (|\sigma^+| - |\sigma^-|)/(|\sigma^+| + |\sigma^-|)$, which leads to $\epsilon = (A^- + A^+) \ln 10/4$, where A^+ and A^- are the amplitudes of light for left- and right-hand circular polarizations. The difference in these amplitudes is referred to as *circular dichroism* (CD). Because this difference is due to resonant absorption or scattering, it is the preferred chiroptical method at wavelengths corresponding to a molecular energy transition or the plasmon resonance. In molecular materials, it is typically of the order of 0.1% and it is useful mainly on molecules having stereocenters in close proximity to chromophores.

The timescales of the ORD and CD processes are very fast, associated with times for light to scatter or be absorbed (10^{-14} to 10^{-15} s). In molecules, their strength is related to the *Rotatory Power* $R_{ab} = \mu_{ab} \cdot m_{ba}$, where a and b are molecular states, μ is the electric dipole transition moment and m is the magnetic dipole transition moment. For ORD and CD to occur, μ and m must have components parallel to each other. This does not occur for symmetric molecules and even in chiral molecules

the effects are small. Enantiomers have opposite sign of m and therefore of R_{ab} and thus their ORD and CD spectra have opposite signs from each other. In real molecules, one must sum over all the states, not just a and b . Because nonlinear optical phenomena are governed by high rank tensors, the information content in the signal is different, and in some cases, more powerful than in linear spectroscopy.^[77]

3.2. Nonlinear Chiroptical Effects

In the linear optical regime, the induced polarization (\mathbf{P}) is linearly proportional to the electric field of light and is written as $\mathbf{P} = \chi^{(1)} \cdot \mathbf{E}$, where the proportionality term $\chi^{(1)}$ is the linear electric susceptibility. For more intense electromagnetic fields however higher harmonics appear in the expression:

$$\mathbf{P} = \chi^{(1)} \cdot \mathbf{E} + \chi^{(2)} : \mathbf{E}\mathbf{E} + \chi^{(3)} : \mathbf{E}\mathbf{E}\mathbf{E} + \dots \quad (3)$$

where $\chi^{(2)}$ and $\chi^{(3)}$ are nonlinear susceptibilities associated with the emission of light at the second and third harmonic, respectively. Because the second harmonic term is the first of the nonlinear expansion, it often gives rise to the largest nonlinear optical signals. The second-harmonic response can be described by a nonlinear polarization, which is expressed in the electric-dipole approximation as:^[78]

$$P_i^{NL}(2\omega) = \chi_{ijk}^{(2)} : E_j(\omega) E_k(\omega) \quad (4)$$

where ω is the frequency of light, $\chi^{(2)}$ is the second order susceptibility tensor, $\mathbf{E}(\omega)$ is the electric field component of the incident light and i, j, k are the Cartesian indices. Upon applying inversion symmetry to this equation, all Cartesian indices change their sign and, therefore, all vectors in Equation 4 change their sign. It follows that:

$$-P_i(2\omega) = \chi_{ijk}^{(2)} : (-E_j(\omega)) (-E_k(\omega)) = P_i(2\omega) = 0 \quad (5)$$

In other words, within the dipole approximation, the second harmonic generation process is forbidden in all materials that are left invariant under inversion symmetry; that is to say, the centrosymmetric materials. Because centrosymmetry is broken at surfaces and interfaces the technique is surface/interface-sensitive down to atomic monolayers. Centrosymmetry is additionally broken by externally applied electric^[79] and magnetic^[80] fields, which makes it possible to image ferroelectric^[81] and ferromagnetic^[82] domains with SHG. In the case of the latter, the SHG dependence on magnetization is due to breaking the time-reversal symmetry, though it should be noted that the SHG signal is not always linear with the magnetization.^[83] Centrosymmetry is also broken by the presence of chirality, which breaks the mirror symmetry of materials. The nature of the symmetry breaking that gives rise to SHG is reflected in $\chi^{(2)}$.

The nonlinear susceptibility $\chi^{(2)}$ is a third rank tensor with 27 components, which can be viewed as a three-dimensional matrix, as in the familiar Rubik cube where each individual sub-cube can be identified by a combination of the three Cartesian indices, as shown in Figure 4d. The number of independent susceptibility components is reduced by a third due to Equation 4, which shows that the last two indices must

be freely permuted since they originate from the same beam within the experimental configuration of Figure 4d. Moreover, depending on the symmetry of the material, the number of non-zero susceptibility components can be further diminished. For example, in the case of an in-plane isotropic sample (with $C_{\infty v}$ symmetry), there are only 3 non-vanishing components and the second order susceptibility becomes:

$$\chi^{(2)} = \begin{pmatrix} 0 & 0 & 0 & 0 & \chi_{xxx} & 0 \\ 0 & 0 & 0 & \chi_{yyz} & 0 & 0 \\ \chi_{zxx} & \chi_{zyy} & \chi_{zzz} & 0 & 0 & 0 \end{pmatrix} \quad (6)$$

where $\chi_{zxx} = \chi_{zyy}$ and $\chi_{xxx} = \chi_{yyz}$. The \hat{x} , \hat{y} , \hat{z} coordinate system is oriented such that the z -axis lays along the sample normal. Should the sample's surface exhibit both in-plane isotropic symmetry and chirality (C_{∞} symmetry), for instance due to a random distribution of chiral molecules or nanoparticles in the x - y plan of the sample, a single additional tensor component appears, $\chi_{xyz} = -\chi_{yxz}$, so that the nonlinear susceptibility tensor becomes:

$$\chi^{(2)} = \begin{pmatrix} 0 & 0 & 0 & \chi_{xyz} & \chi_{xxx} & 0 \\ 0 & 0 & 0 & \chi_{yxz} & \chi_{xxx} & 0 \\ \chi_{zxx} & \chi_{zyy} & \chi_{zzz} & 0 & 0 & 0 \end{pmatrix} \quad (7)$$

Often this additional component is referred to as the chiral one, since it is present only in chiral systems. The other components are referred to as achiral because they occur in both chiral and achiral systems. The chiral component leads to the appearance of nonlinear chiroptical effects, such as SHG-CD and SHG-OR, that are considered nonlinear optical equivalents of the linear CD and OR. However it also results in nonlinear chiroptical effects that have no equivalent in linear optics. In particular, because it is possible to individually select the chiral tensor element (all the others being zero) by the P_{IN} - S_{OUT} polarizer-analyzer combination, any SHG signal that is detected in this configuration constitutes a measure of chirality. Having a single non-zero tensor component greatly simplifies the mathematics and, within the Lorentz model of the susceptibility, we can express $\chi^{(2)}$ in terms of the resonance frequency ω_0 as:^[84,85]

$$\chi^{(2)}(2\omega) = \zeta^{(2)} \frac{Ne^3}{m^2} \frac{1}{(\omega_0^2 - 4i\gamma\omega - 4\omega^2)(\omega_0^2 - 2i\gamma\omega - \omega^2)^2} \quad (8)$$

where $\zeta^{(2)}$ is the first anharmonic term that characterizes the strength of the nonlinearity, N is the electronic number density, e and m are the charge and the mass of the electron, and γ is the damping constant. Equation 8, allows us to perform a relatively simple yet highly selective nonlinear spectroscopy, which has been demonstrated in chiral molecular materials,^[86] yet, to our best knowledge, it has not yet been applied to chiral metamaterials. It should be pointed out however that the method places rather specific requirements on both the experiment and on the samples. By comparison, SHG-CD and SHG-OR are more general.

For the purpose of simplifying the somewhat cumbersome notations of numerous tensor components, a change of coordinate system can be adapted, from the \hat{x} , \hat{y} , \hat{z} sample directions to the directions of principle light polarization and the wave

vector: \hat{S} , \hat{P} , \hat{k} . The second harmonic field can then be written in terms of the S and P components of the fundamental field as:^[87]

$$\mathbf{E}(2\omega) = f E_P^2(\omega) + g E_S^2(\omega) + h E_P(\omega) E_S(\omega) \quad (9)$$

where f , g and h are complex numbers, which are linear combinations of the Cartesian susceptibility tensor components $\chi^{(2)}_{ijk}$. In the following, we shall indicate the real and imaginary part of these complex values by the indices r and i , respectively. The nonlinear Fresnel factors can also be taken into account within the three coefficients in Equation 9. Furthermore, just as in the case of the nonlinear susceptibility, the exact form of f , g and h depends on the symmetry of the sample. In addition, their value can be affected by the angle of optical incidence ψ , the experimental geometry and is different for the S - and P -polarized component of the second harmonic field. Neglecting the refractive indices, for P -polarized fundamental light incident on a chiral isotropic surface and in the reflection geometry, see Figure 4d, the dependence of f , g and h on the different susceptibility tensor components can be recovered:^[88]

$$\begin{aligned} f_S &= -\sin\theta (2\chi_{xyz} \cos\psi) \\ g_S &= 0 \\ h_S &= \sin\psi (2\chi_{xxx}) \\ f_P &= \sin\psi (2\chi_{zzz} \sin^2\psi + \chi_{zxx} \cos^2\psi - 2\chi_{xxx} \cos^2\psi) \\ g_P &= \sin\psi (\chi_{zxx}) \\ h_P &= -\sin\psi (2\chi_{xyz} \cos\psi) \end{aligned} \quad (10)$$

where the subscripts S and P refer to the particular component of the second harmonic field. Thus, for S polarized SHG, the coefficient f is chiral, while g and h are achiral. In contrast, for P polarized SHG, h is chiral, while g and f are achiral. Very similar relations can be derived for the transmission geometry.

The SHG-CD is then written as the difference between the SHG intensity for left- and right-hand incoming circularly polarized light, divided by half the sum. This quantity can be expressed in terms of the complex parameters f , g and h as:

$$\begin{aligned} I_{SHG-CD} &= \frac{I_{LCP}(2\omega) - I_{RCP}(2\omega)}{\frac{1}{2}(I_{LCP}(2\omega) + I_{RCP}(2\omega))} \\ &= \frac{4[(f_i - g_i)h_r - (f_r - g_r)h_i]}{|f|^2 + |g|^2 + |h|^2 - 2(f_r g_r + f_i g_i)} \end{aligned} \quad (11)$$

This equation shows that SHG-CD is due to an interference between the achiral and the chiral susceptibility components. It follows that a large SHG-CD signal requires that the chiral and achiral coefficients be of similar magnitude. This is not the case for SHG-OR.

For P -polarized input, and choosing $\psi = 45^\circ$, the SHG-OR can be written as:^[88]

$$|\phi|_{SHG-OR} = \tan^{-1} \left(\frac{|f_S|}{|f_P|} \right) = \tan^{-1} \left(\frac{|h_P|}{|f_P|} \right) \quad (12)$$

where we see directly a ratio between chiral and achiral coefficients. Consequently, a large SHG-OR requires a large chiral contribution to the SHG signal as well as a small achiral one.

Generally speaking, all the nonlinear chiroptical effects can benefit from the large field amplitudes of ultrafast laser pulses and the strong near-field enhancements of localized surface plasmon resonances. It should be pointed out though that these enlargements have limits. For instance, at laser fluence of 2.7 mJ/cm², gold nanostructures can be damaged.^[89] Moreover, the local near-field enhancements, such as those generated between two plasmonic nanoparticles cease to increase upon entering the quantum regime, at separation distance of 0.3 nm.^[90]

4. Giant Chiroptical Effects

4.1. Giant Chiroptical Effects in Linear Optics

Giant optical rotation was first reported from arrays of chiral gold nanostructures, whose geometry can be seen in the scanning electron micrographs of Figure 5. The nanostructures were grown by electron beam lithography, see Figure 2. The pitch of the array is 500 nm and the line width is 80 nm. These nanostructures consisted of 95 nm thick Au layer, capped with 23 nm Cr. Despite being very thin, compared to the plasmon resonance wavelength, these arrays produced chiroptical effects of magnitude equivalent to chiral molecular materials several orders of magnitude thicker. More specifically, Figure 5a shows the angle of optical rotation Δ upon azimuthal rotation of the sample, measured by the angle ϕ . A clear offset can be observed, denoted θ . This offset disappears for the achiral array in Figure 5b and it reappears with an opposite sign in Figure 5c, where the array has an opposite chirality to the initial one. The offset θ indicates the difference in effective absorption coefficient for the two circularly polarized components of linearly polarized light. Upon calculating the optical rotation as a function of the thickness of the nanostructures, a value of approximately 10⁴⁰/mm is obtained, which can indeed be considered as giant. It should be pointed out that, despite being generally referred to as 2D, in fact these nanostructures are not. Indeed, a true 2D chiral nanoarray would reverse its chirality upon flipping the array around, as this operation would be equivalent to a mirror reflection. The experiment performed on these arrays however demonstrated that chirality is preserved upon flipping the sample around. Consequently, it is the difference between the Cr/Au and the Au/substrate interfaces that endows the array with three-dimensional chirality.

Recently, giant chiroptical effects were reported from plasmonic nanostructures of much more pronounced three-dimensionality. The inset in Figure 5d, shows the same gold gyroid geometry, whose preparation from block copolymers was shown in Figure 2. In the inset of Figure 5d, the gyroid is represented as viewed from the [111] direction, which reveals a chiral spiral along the network. The unit cell of this network is 50 nm, and the thickness of the gold struts is 10 nm. Because the entire network is 200 nm thick, the chiroptical effect that was measured could also be qualified as giant. The second inset in Figure 5d, presents the experimental geometry, whereby the sample was tilted by 35° and subsequently rotated around the surface normal. In the plot, the gyrotropic transmission ΔT ,

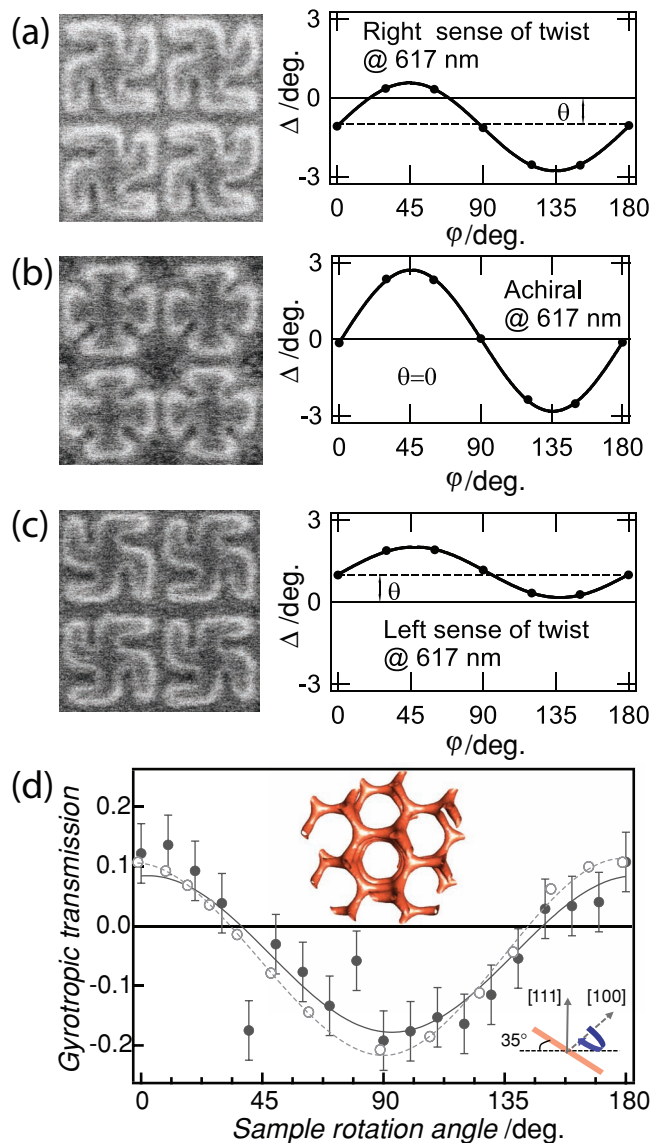


Figure 5. Giant linear chiroptical effects have been observed for both 2D and 3D chiral nanomaterials. In (a), for left-hand twisted 2D gratings, the polarization azimuth rotation angle Δ reveals an offset θ , which is a measure of chirality.^[91] In (b), for the achiral gratings, it can be seen that θ is zero. Whereas in (c), for the right-hand twisted gratings, the sign of θ has similar value and opposite sign to that in (a). Although small in absolute value, the optical activity in these nanomaterials is very large compared to that of similarly thick natural materials. In (d), Gyrotropic transmission through a 3D sample inclined at 35°. The gyrotropic transmission is the difference between the transmission spectra in left and right channels as the sample was rotated around the [110] axis. The open symbols are the results of a finite difference time domain calculation, while the full ones are the measurements. Lines are guides for the eye. Panels (a-c) adapted with permission from Ref. 54. Copyright 2005, American Physical Society. Panel (d) reproduced with permission from Ref. 67. Copyright 2012, Wiley.

i.e., the normalized difference in sample transmission for left- and right-hand circularly polarized light, is shown as a function of sample rotation angle. The wavelength of light covered the region 600 to 750 nm and was averaged. The transmission of

circularly polarized light is maximal for the two rotation angles (0° and 180°) where the optical axis is collinear with the $[111]$ and $[\bar{1}\bar{1}\bar{1}]$ directions. By varying the rotation angle, the optical path is increasingly obstructed by Au struts, reducing $|\Delta T|$. The rotation of the sample therefore leads to the clear observation of chirality in this gyroid metamaterial. The measurement data were further confirmed by a finite difference time domain simulation.

To summarize, in linear optics, giant chiroptical effect can be observed from nanostructured materials that have been assembled both through the top-down and the bottom-up nanotechnological approaches. In chiral molecular materials, nonlinear chiroptical effects are typically three orders of magnitude larger than their linear optical counterparts. In the next section, we shall examine the nonlinear chiroptical effects in plasmonic nanomaterials and discuss their values with respect to the giant linear ones.

4.2. Giant Chiroptical Effects at the Second Harmonic

Let us consider the arrangements of chiral G-shaped nanostructures in Figure 6a. For clarity, the borders of the nanostructures in the scanning electron micrograph have been highlighted in yellow. The samples were prepared by electron beam lithography and consist of gold; more details on the exact experiment can be found in Ref. [56]. Figures 6b and 6d show SHG microscopy images. SHG microscopy has a well known sensitivity to local field enhancements and can be performed in a variety of experimental geometries.^[92–97] The images in Figure 6 were acquired upon scanning the laser on the surface of the samples with two opposite directions of circularly polarized light, in Figure 6b and 6c, respectively. Depending on the direction of circularly polarized light, it can then be seen that the pattern of SHG emission differs significantly. Additionally, in the case of the mirror-G-shaped nanoparticles (Figure 6d) this difference in SHG emission pattern reverses, as demonstrated in Figure 6e and 6f. The pattern of SHG emission can be related to hotspots in the near-field enhancements. Consequently, in the case of G-shaped and mirror-G-shaped nanostructures, the chirality, which is observed in the microscopic SHG, can be attributed to a chiral coupling between the four Gs at the centre of each unit cell.

Figure 6g shows a plot of the SHG intensity as a function of quarter wave plate rotation for the G-shaped and mirror-G-shaped gold nanostructures. There are four peaks, at the angles for which the quarter wave-plate produces exactly circularly polarized light. For emphasis, in the figure, these angles have been marked with oriented circles. It is immediately apparent that there is a difference between the size of the peaks, depending on the direction of circularly polarized light and the handedness of the samples, which is a clear signature of chirality.

In linear optics, the CD effect is typically evaluated as the difference in transmission for left- and right-hand circularly polarized incident light. SHG-CD can be evaluated in a similar configuration, as the difference in *forward* generated second harmonic light, for left- and right-hand circularly polarized incident light. For instance, in such an experiment, 15% forward

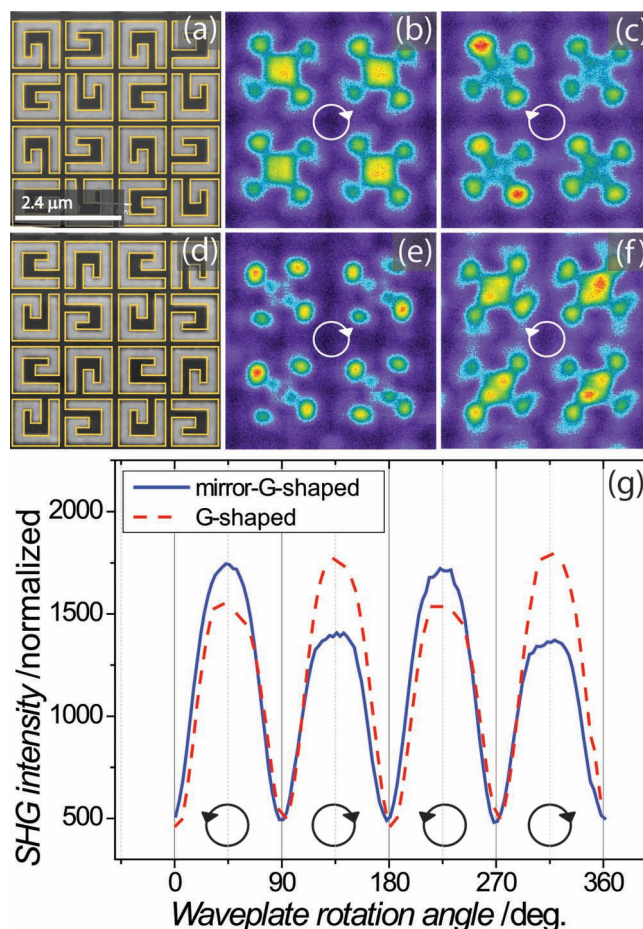


Figure 6. Giant chiroptical effects can be observed in second harmonic generation. In (a), an SEM picture of G-shaped nanostructures is presented. The yellow lines have been added around the edges of the structures in order to improve the visibility. In (b), an SHG micrograph obtained for right-hand circularly polarized light is presented. In (c), an SHG micrograph obtained for left-hand circularly polarized light is shown. There is a clear difference in the SHG hotspot pattern depending on the direction of circular polarization. Moreover, as is clear from figures (d), (e) and (f), this difference depends on the handedness of the nanostructures. In (g), SHG-circular dichroism data demonstrate that the properties of the hotspot patterns translate into effective far-field properties of the entire nanostructured surface. The data present the SHG intensity as a function of the angle of quarter wave plate rotation; the wave plate positions for left- and right-hand circularly polarized light are indicated with oriented circles.^[56] Adapted with permission from Ref. 56. Copyright 2009, American Chemical Society.

SHG-CD was reported from a combination of two 25 nm thick twisted crosses, illuminated at the wavelength of 1060 nm. It should be pointed out though that, despite the strong values that can be obtained in the transmission/forward geometry, the strong absorption of the materials constitutes an important limitation.

Because the SHG signal is dominantly generated from the surfaces and interfaces, where the plasmonic field enhancements occur, a strong SHG-CD signal can be measured in the reflection geometry as well, i.e., for *backward* generated second harmonic light. Reflection geometry is particularly important

because it constitutes a convenient probe for molecules at the surface of plasmonic nanostructures. In the 25 nm thick G-shaped nanostructures presented here, the backward SHG-CD reaches 10%. And over 40% backward SHG-CD was reported in star-shaped gold nanostructures with thickness 30 nm, at the wavelength of 800 nm. In both linear and nonlinear chiroptical experiments though, additional factors can have an influence on the magnitude of the measured effects.

4.3. Pseudo/Extrinsic Chirality

In 2009, strong chiroptical effects were reported from a photonic metamaterial,^[62] where the unit cells were not intrinsically chiral. The nanostructures in this metamaterial were made of Al, had a thickness of 50 nm, and, at the wavelength of 1100 nm, exhibited up to 7% circular dichroism. The chiroptical behaviour appeared at oblique incidence, it reversed sign upon reversing the sign of the incidence angle and it disappeared at normal incidence. It was suggested that the wave vector \hat{k} , the surface normal \hat{n} and the light polarization vector \hat{S} constituting a chiral triad were responsible for this type of *extrinsic chirality* in split ring metamaterials. Later, these findings were generalized as it was demonstrated that planar metamaterials that rely on a single resonance to achieve a simultaneous electric and magnetic response always exhibit a strong optical activity, regardless of whether they are chiral or not. It was also recognized that, in molecular materials, this type of chiroptical behaviour had already been referred to as *pseudochirality*, and had, for instance, been observed with SHG in 1996. Very recently, pseudo/extrinsic chirality at the second harmonic was also demonstrated in plasmonic nanostructured materials.

In Figure 7, the first column indicates the geometry and sample orientation with the symbols corresponding to the measurements (blue circle or red square). Second column: 3D schematics of the samples' orientation are shown together with the direction of \hat{k} (solid blue arrow), \hat{n} (dotted black arrow), \hat{R} (dashed red arrow), and the preferential direction of the induced current density J (curved black arrow). Third column: the nonlinear optical measurements. In (a), SHG-CD of the sample with straight nanowires for 0° (blue circles) and 180° (red squares) orientation of the sample. In (b), SHG-CD of the sample with curved nanowires for 0° (blue circles) and 180° (red squares) orientation of the sample. The two lines are fitting curves. In (c), SHG-CD of the sample with curved nanowires for 90° (blue circles) and 270° (red squares) orientation of the sample. Fourth column: the schematics of the sample orientation at the end of the experiments. Adapted with permission from Ref. 63. Copyright 2011. American Physical Society.

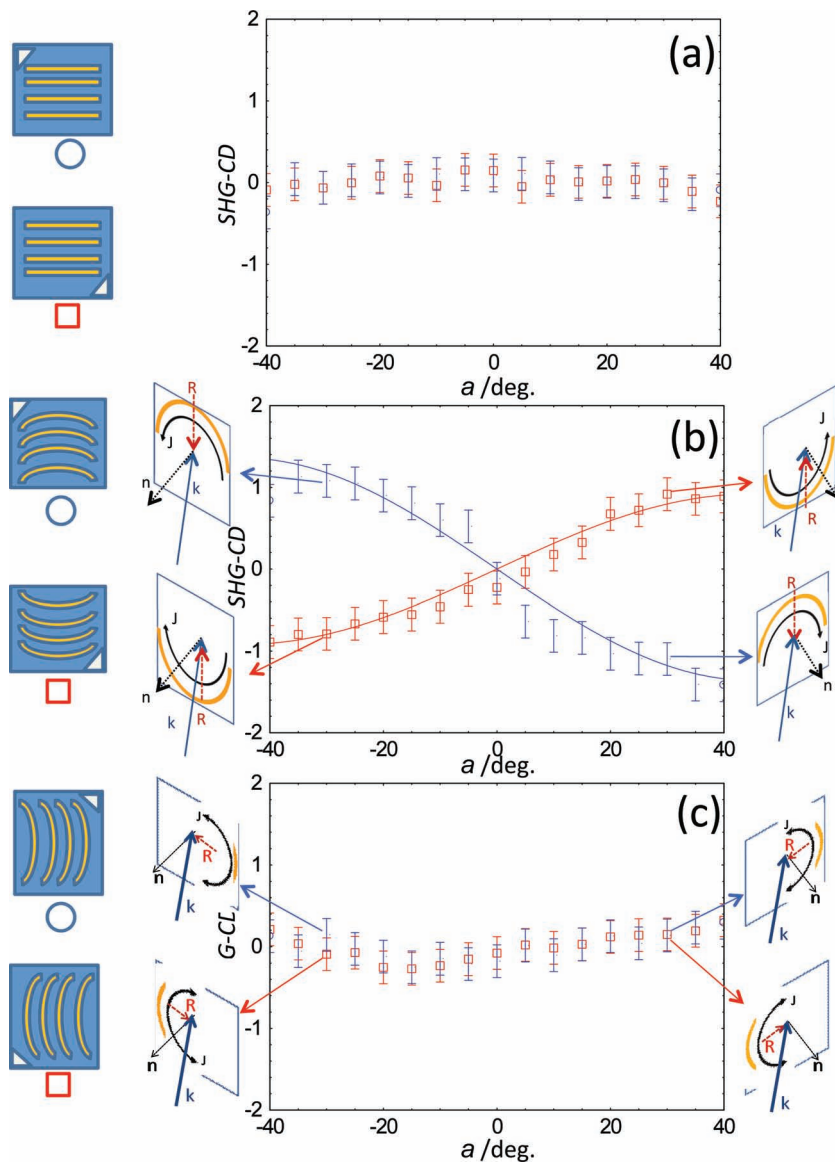


Figure 7. Chiroptical effects can be observed due to the presence of chirality in the experimental geometry. Left column: 2D schematics of the samples' orientation with the symbols corresponding to the measurements (blue circle or red square). Second column: 3D schematics of the samples' orientation are shown together with the direction of \hat{k} (solid blue arrow), \hat{n} (dotted black arrow), \hat{R} (dashed red arrow), and the preferential direction of the induced current density J (curved black arrow). Third column: the nonlinear optical measurements. In (a), SHG-CD of the sample with straight nanowires for 0° (blue circles) and 180° (red squares) orientation of the sample. In (b), SHG-CD of the sample with curved nanowires for 0° (blue circles) and 180° (red squares) orientation of the sample. The two lines are fitting curves. In (c), SHG-CD of the sample with curved nanowires for 90° (blue circles) and 270° (red squares) orientation of the sample. Fourth column: the schematics of the sample orientation at the end of the experiments. Adapted with permission from Ref. 63. Copyright 2011. American Physical Society.

and \hat{R} that gave rise to the effect. The idea was tested in a control experiment, Figure 7c, where it is clear that the SHG-CD disappears whenever \hat{R} is perpendicular to the cross product of \hat{k} and \hat{n} . Based on these observations, a phenomenological equation for the SHG-CD was suggested:

$$\frac{I_{LCP}(2\omega) - I_{RCP}(2\omega)}{I_{LCP}(2\omega) + I_{RCP}(2\omega)} = \frac{\alpha}{R} \hat{R} \cdot (\hat{k} \times \hat{n}) \frac{P^2(\omega)}{A} (\hat{k} \cdot \hat{n}) \quad (13)$$

where P is the input power at the fundamental frequency, A is the spot size area and α is a constant. Within this expression, the term $\frac{P^2(\omega)}{A} (\hat{k} \cdot \hat{n})$ accounts for the enlargement of the spot size at larger incidence angle. In these experiments, for P polarized light, estimates of the SHG-CD value reached 54%. It is therefore quite clear that, for both linear and nonlinear optics, chiroptical effects are not only sensitive to the chirality of the material but also to the geometry of the experiment. This is why universal measures of chirality are hard to define and assess. Next, we shall see how the chirality of light itself can be used to increase the chiroptical phenomena.

4.4. Superchiroptical Effects

We have already seen that for circularly polarized light, the electric field vector rotates as the light wave propagates. Let us consider the 2,2'-dimethoxy-binaphthyl molecule in Figure 1g upon illumination by circularly polarized light. Suppose that initially the electric field vector is along one arm of the molecule. For a maximal chiroptical effect, we would like that, by the time the wave reaches the second arm, its electric field is situated along the direction of the second arm. Unfortunately, whereas the distance between the two arms is <1 nm, the helical pitch of circularly polarized light is 400 to 800 nm. By comparison, a better fit to the helical pitch of circularly polarized light can be achieved in nanostructures that are built upon the principle of chiral coupling from achiral elements, which are much larger than molecules. A successful strategy for enhancing chiroptical effects consists therefore in trying to match the helical pitch of light with that of the nanostructures. A much more flexible strategy might be to match the helical pitch of light to that of the nanostructures or molecules, thereby achieving superchiral light.^[50]

For circularly polarized light, the dissymmetry factor, g_{CPL} , is a measure for the rates of excitation between left- and right-hand circularly polarized light. This concept can be generalized beyond the special case of circularly polarized light by the following expression for the dissymmetry factor:

$$g = g_{CPL} \left(\frac{cC(r)}{2U_e\omega} \right) \quad (14)$$

where c is the speed of light, ω is the angular frequency, U_e is the local density of electron states and $C(\mathbf{r})$ is the optical chirality, which is defined as:

$$C(r) = \frac{\epsilon_0}{2} E(r) \cdot (\nabla \times E(r)) + \frac{1}{2\mu_0} B(r) \cdot (\nabla \times B(r)) \quad (15)$$

It follows that if one could enhance $C(\mathbf{r})$, the chiroptical effects in materials would also be enhanced. Superchiral fields have thus been employed to achieve 11-fold chiroptical enhancements, by means of a standing wave pattern. Strong optical chirality can also be achieved in the vicinity of chiral plasmonic nanostructures and several such patterns have been analyzed and design principles have been proposed.^[98]

So far we have seen that giant chiroptical effects can be observed in plasmonic nanostructures. Because the plasmonic local field enhancements are located at the surface of the nanostructures, surface-specific methods for chiroptical characterization, such as SHG, also achieve giant values. In linear optics, chiroptical effects arise due to the interaction between electric and magnetic field of light. In metamaterials, these electric and magnetic fields can be locally enhanced to a similar magnitude, which favours very strong coupling coefficients and therefore large chiroptical effects, with or without actual chirality in the nanostructures. Moreover the helical pitch of circularly polarized light can be compressed in the vicinity of plasmonic nanoparticles to achieve local superchiral light, which significantly increases chiroptical interactions. In all of these methods, plasmonics plays a crucial enabling role. While all of the methods can be used to reach giant chiroptical effects, different combinations can yield even larger chiroptical responses. It is already possible to detect the chirality of single molecules.^[99] By implementing combinations of strong chiroptical effects, we believe that soon the manipulation of single chiral molecules with light will become widespread. When it comes to manipulation, switches will very likely play a key role in future developments. In the next section, we shall present two examples of switching chiroptical behaviour.

5. Outlook

Upon interacting with molecules, plasmonic chiral nanomaterials can find numerous possible applications, such as sensing, imaging and enantioselective reactions. Building upon the geometric and electromagnetic interplay between plasmonic and organic chiral nanomaterials, hybrid materials with novel linear and nonlinear chiroptical properties may be assembled. Upon incorporating DNA and viruses within such hybrid materials, bio-functionalities could be achieved, thereby opening the way for new medical procedures and perhaps even artificial life. In the near-future, we expect that active, or switchable, chiral nanostructures will play an increasingly important role, together with chiral optical metamaterials.

5.1. Chiral Metamaterials

In chiral metamaterials, the constitutive relations are $\mathbf{D} = \epsilon_r \epsilon_0 \mathbf{E} + i\xi \sqrt{\mu_0 \epsilon_0} \mathbf{H}$ and $\mathbf{B} = \mu_r \mu_0 \mathbf{H} - i\xi \sqrt{\mu_0 \epsilon_0} \mathbf{E}$, where \mathbf{D} is the electric displacement field, \mathbf{B} is the magnetic induction field, \mathbf{E} and \mathbf{H} are the electric and magnetic field respectively, ϵ_r and ϵ_0 are the relative permittivity and the permittivity of vacuum, μ_r and μ_0 are the relative permeability and the permeability of vacuum while ξ is the chirality parameter. This parameter increases the refractive index of light for one direction of circularly polarized light (n^+) and it decreases the refractive index of light for the other (n^-), so that $n^\pm = n \pm \xi$, where $n = \sqrt{\epsilon_r \mu_r}$. Consequently, a large $|\xi|$ leads directly to negative refractive index for one of the circularly polarized electromagnetic waves in chiral metamaterials. By enabling negative refractive index, chiral metamaterials could therefore lead to advances in optical nanolithography, superlensing and fully

light-based nanocircuits. In all of these cases, the chirality within metamaterials interacts with the helicity of the polarization vector of light. Light however can also propagate with a helical phase front.

In Laguerre-Gaussian beams, a vortex in the phase front can endow the light with orbital angular momentum. Theoretically, it has been shown that this orbital angular momentum of light cannot interact with the internal states of molecules through an electric-dipole mechanism.^[100] Experimentally, it has also been demonstrated that Laguerre-Gaussian beams do not display chiroptical effects in molecular materials.^[101] With respect to metamaterials though, recently, Laguerre-Gaussian beam carrying both orbital and spin angular momentum have been employed to control the chirality in twisted metal nanostructures.^[102] In these experiments, laser ablation with Laguerre-Gaussian beams was performed and the helicity of the beam was transferred to the melting metal resulting in the formation of chiral nano-needles. Although the overall size of the light matter interaction in these experiments extended over 25 μm , it has been revealed that similar though achiral nano-needles, or nanojets, can occur within 200 nm with the help of plasmonic hotspots.^[89]

Through their interaction with complex light, the complex geometries of chiral metamaterials can lead to novel scientific and technological breakthroughs; for instance, based on novel spin-orbit exchange mechanisms, nonlinear behaviour and opto-manipulation of chiral states.^[103]

5.2. Switching the Handedness of Chiral Local Field Enhancement with Circularly Polarized Light

In Figure 8a, we consider square-ring-shaped gold nanostructures. For linearly polarized illumination, the charges are driven along the direction of linearly polarized light and, consequently, near-field enhancements, or hotspots, are produced, see Figure 8a. For circularly polarized light though, there is no privileged direction and consequently, there should be no hotspots. Instead, the charges can be expected to distribute more or less homogeneously on the surface of the square ring, as schematically indicated in Figure 8. This hypothesis was tested by means of SHG microscopy imaging, which was performed on arrays of gold square-rings, with linear and circularly polarized light, in Figure 8c and 8d, respectively.^[104] The SHG microscopy shows that in the former case, there are pairs of clearly resolvable hotspots, which match the neighbouring sides of the squares that are oriented perpendicularly to the direction of linearly polarized

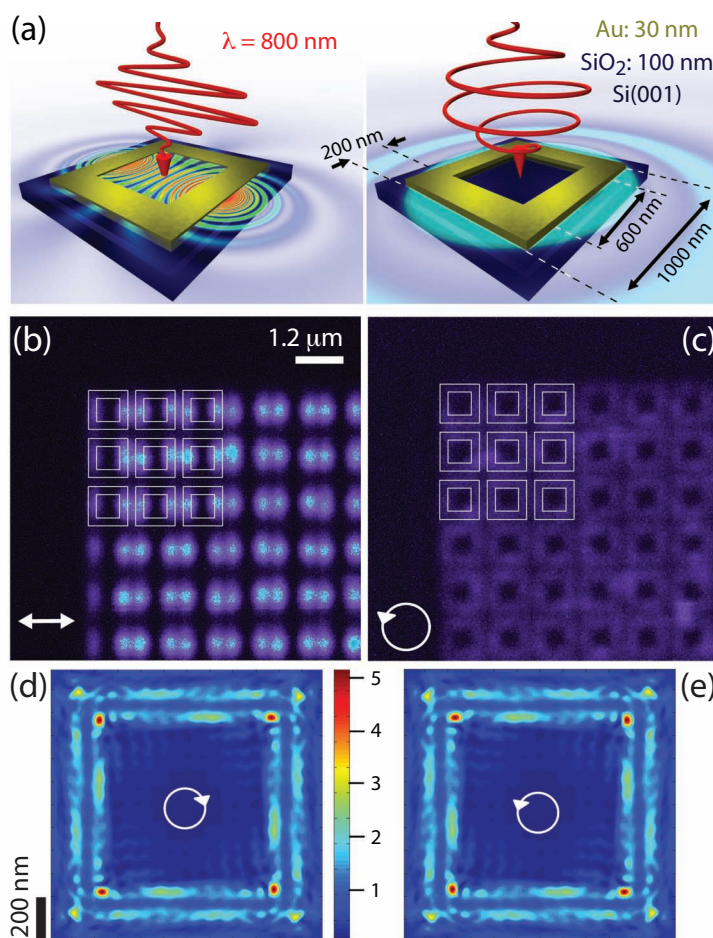


Figure 8. Switching the handedness of chiral local field enhancements. (a) Schematic of SHG emission from square-ring gold nanostructures depending on the polarization state of light. In response to linearly polarized incident light, near-field enhancements of the electric field cause SHG hotspots on the surface. For circularly polarized incident light, the electric near-field enhancements cause more homogeneous SHG emission from the surface of the nanostructures. In (b), SHG microscopy pictures for horizontal linearly polarized light reveal hotspots that are arranged along the direction of polarization. In (c), SHG microscopy for circularly polarized light shows a homogeneous SHG response from the surface of the square-rings.^[104] In (d) and (e), numerical simulations of the electric near-fields in a plane immediately above the air/gold interface. The state of polarization is indicated with white arrows. Adapted with permission from Ref.^[104]. Copyright 2012. Wiley. John and Sons.

light. In the case of circularly polarized light, the squares can be resolved entirely, due to the homogeneous distribution of the field enhancements. Because these square-rings are achiral, the SHG microscopy shows no difference in the images recorded for left- and right-hand circularly polarized light. However, it should be noted that the image of Figure 8c is at the limit of the optical resolution that can be achieved with SHG microscopy. To gain further understanding of the effect of circularly polarized light on the electron density of the nanostructures, numerical simulations can be performed providing suitable nanoscale resolution.

Figure 8d and 8e show the electric field enhancements at a distance of 1 nm above the nanostructure, for the two directions of circularly polarized light. The simulation results are in

good agreement with the experiments, see Ref. [104], but indicate something more. Upon examining the pattern of the local field enhancements, we note that they exhibit a sense of rotation, i.e., they are chiral. Moreover, their handedness reverses upon reversing the direction of circularly polarized light. These simulations of the near-fields were performed with RSoft's Diffract MOD software and their conclusions were also supported by independent simulations of the local electric currents, at the depth of 1 nm below the surface of the nanostructures. The simulations of currents were performed with the MAGMAS Maxwell equations solver. Because the squares are definitely achiral, the only explanation for the appearance of chirality in the simulation results is that the chirality of light itself has been imprinted on the local currents and near-field distribution. It is therefore possible to use circularly polarized light, to bestow chirality upon achiral nanostructures and to switch that chirality by switching the direction of circularly polarized light. Such chiral switches could potentially be used to manipulate chiral molecules in the vicinity of the nanostructures. Whereas in this example the chirality of light switches the handedness of the nanostructures, in the next section we shall see how the handedness of the nanostructures could be used to switch the sign of the chirality of light.

5.3. Switching Optical Activity

In molecular materials, switching the handedness of chiral molecules is well known in chemistry and it can be performed by various methods, for instance by photoexcitation, redox changes, electron tunneling, temperature variations, solvent strength and pH control. In order for chiral switches to be efficient, the speed of chiral interconversion is essential. For this reason, electro-active organic polymers, such as polyaniline, whose helical conformation can be modulated by reduction and oxidation are sought after.^[105] Moreover, optical switching, that can be performed at wavelengths different from that at which chiroptical effects are measured, might be of interest for data recording. Such photoswitchable molecules are helical-shaped overcrowded alkenes and diastereomeric bistable molecules.^[106] However, the typically small values of chiroptical effects in molecules constitute an important limitation.

Recently, the switching of chiroptical effects in terahertz metamaterials has been shown to achieve optical rotation in excess of 10° for a single metamaterial layer.^[107] The geometry of the structures is shown in Figure 9a and Figure 9b. The lateral dimension of the unit cell is $50\ \mu\text{m}$. The unit cell is composed of structures with opposite handedness (A and B), which unmodified simply cancel each other's chiroptical contributions. The

architectures used in Figure 9 however were modified. The structures are built upon a silicon-on-sapphire substrate, in a manner that incorporates silicon pads in the chiral three-dimensional design. In A, the isolating pad bridges two already separate parts of the structures. As a consequence, A is virtually unmodified. In B however, the pad replaces part of the metallic architecture with an isolator and therefore the resonance red-shifts. Following the insertion of these pads, at the original resonance frequency, the structure now exhibits a net chiroptical response, which is due to A (as B is red-shifted). Moreover, the chiroptical response can be switched upon illumination by an ultrafast laser operated at the wavelength of 800 nm (50 fs, 1 kHz repetition rate). Indeed, at this wavelength, the charges in Si are excited above the band-gap, and as a consequence, the pads become conductive. The effect upon A is dramatic, as the previously unconnected parts of the structure are suddenly shortened. Henceforth, the resonance in A is virtually suppressed. Conversely, B, which was shortened by the isolating Si, finds itself essentially restored to its original dimensions by the change in conductivity. Overall,

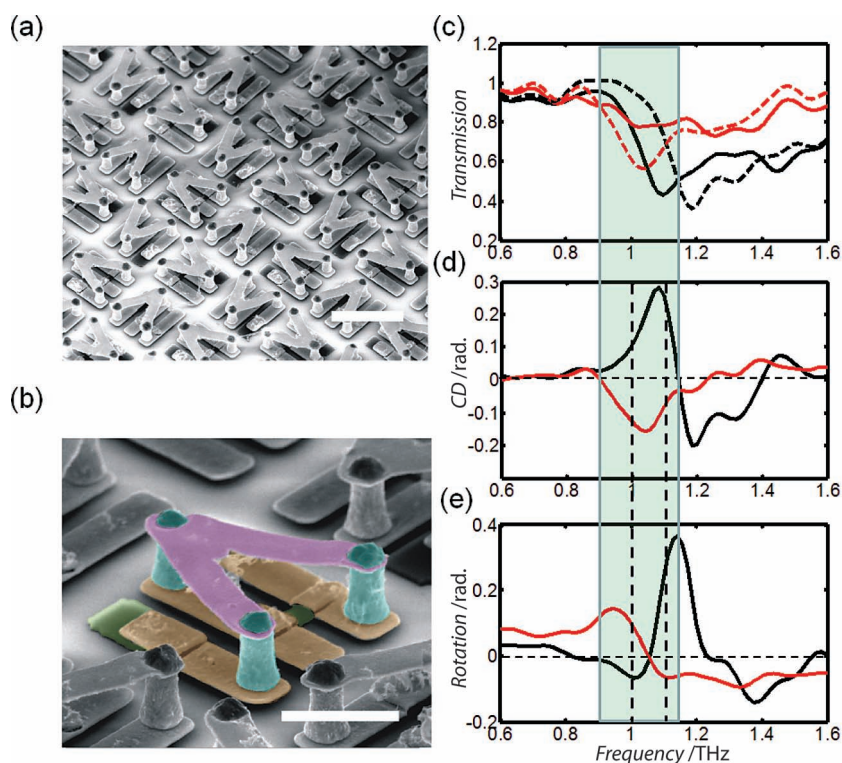


Figure 9. The handedness of the structures can be used to switch the sign of chiroptical effects. In (a) and (b), scanning electron microscopy images of the fabricated metamaterial. The period of the metamaterial is $50\ \mu\text{m}$ and the scale bar in (a) is $25\ \mu\text{m}$. In (b), the purple, blue and yellow colours represent the gold structures at different layers and the two silicon pads are shown in green. The scale bar measures $10\ \mu\text{m}$. In (c), the measured transmission spectra for left- (solid) and right-hand (dashed) circularly polarized light, without (black) and with (red) photoexcitation. The shaded region represents the frequency range where the relative transmission amplitude between left- and right-hand circularly polarized light is reversed. In (d) and (e), the CD spectrum and ORD derived from the measured transmission amplitude and phase spectra are shown, respectively. The curves correspond to transmission without (black) and with (red) photoexcitation. In the shaded area, both the signs of CD and ORD are flipped, indicating the switching of handedness of the metamolecules. Adapted with permission from Ref. 107. Copyright 2012, Nature Publishing Group.

the photoexcitation causes a net chiroptical response to appear, this time due to B , (as A is shortened). The range over which the chiroptical response can thus be switched by turning on and off the photoexcitation extends from 0.9 to 1.14 THz.

6. Summary

To summarize, very large chiroptical effects have recently been achieved from chiral plasmonic nanostructures. These accomplishments are mainly due to the development of bottom-up and top-down approaches for material design and fabrication at the nanoscale. Both giant linear and nonlinear chiroptical values have been reported. For the linear case, chiroptical effects originate in the local coupling between electric and magnetic fields. In nanostructures, while the localized surface plasmons can efficiently enhance both the electric and the magnetic field of light, the geometrical confinement can efficiently couple the fields. For the nonlinear case, chiroptical effects can exist solely within the electric dipole approximation. Large chiroptical values can therefore arise from the surface-sensitivity of the techniques and because, as their name indicates, localized surface plasmons lead to enormous electromagnetic field enhancements precisely on the surface. Besides the chirality of the nanostructures, chiroptical effects can be enhanced by making use of the experimental geometry and of the chirality of light itself. We believe that further optimization can be achieved by combining different types of chiral enhancements. In particular, the helical pitch of circularly polarized light could be manipulated by using the local fields of plasmonic nanostructures to match the helical pitch of molecules. Moreover, because the chiroptical response of molecules is typically in the UV range, whereas that of plasmonic nanoparticles is in the visible and near-IR, nonlinear (multiphoton) processes could be used to efficiently couple the two spectral regions. We believe that development and understanding of the chiroptical effect in plasmonic nanostructures will lead to unprecedented levels of chiroptical sensitivity for molecules and will also allow efficient asymmetric molecular synthesis and catalysis. In the future, chiroptical switches will very likely play an important role in technological applications of chiral plasmonic nanostructures. It has already been shown that switching the chirality of incoming light can cause a reversal of the handedness in the nanostructures. Additionally it has also been demonstrated that switching the handedness of the nanostructures can cause a reversal in the chirality of outgoing light. Although the latter was demonstrated at terahertz frequencies, transposing its principle to the optical frequency is only a matter of time.

Acknowledgements

We acknowledge financial support from the EPSRC grant EP/G060649/1, the KU Leuven (CREA, GOA), the FARI project supported by Roma University and the MARINE project supported by the Italian Ministry of Defence.

Received: December 17, 2012

Revised: January 30, 2013

Published online: April 2, 2013

- [1] Lord Kelvin, in *Baltimore Lectures on Molecular Dynamics and the Wave Theory of Light*, Clay and Sons: London, **1904**, p.449.
- [2] S. A. Maier, in *Plasmonics: Fundamentals and Applications*, Springer, **2007**.
- [3] K. H. Dostert, M. Álvarez, K. Koynov, A. del Campo, H. J. Butt, M. Kreiter, *Langmuir* **2012**, *28*, 3699–3703.
- [4] T. Chen, H. Wang, G. Chen, Y. Wang, Y. Feng, W. Shan Teo, T. Wu, H. Chen, *ACS Nano* **2010**, *4*, 3087–3094.
- [5] A. Nitzan, L. E. Brus, *J. Chem. Phys.* **1981**, *75*, 2205–2214
- [6] C. J. Chen, R. M. Osgood, *Phys. Rev. Lett.* **1983**, *50*, 1705–1708.
- [7] M. I. Stockman, *Top. Appl. Phys.* **2006**, *103*, 47.
- [8] K. Kneipp, Y. Wang, H. Kneipp, L. T. Perelman, I. Itzkan, R. R. Dasari, M. S. Feld, *Phys. Rev. Lett.* **1997**, *78*, 1667.
- [9] S. Nie, S. R. Emory, *Science* **1997**, *275*, 1102.
- [10] Y. Inoue, V. Ramamurthy, in *Chiral Photochemistry*, Marcel Dekker: New York, NY, **2004**.
- [11] S. Knoppe, I. Dolamic, A. Dass, T. Burgi, *Angew. Chem. Int. Ed.* **2012**, *51*, 7589–7591.
- [12] C. Noguez, I. L. Garzón, *Chem. Soc. Rev.* **2009**, *38*, 757–771.
- [13] V. Kitaev, *J. Mater. Chem.* **2008**, *18*, 4745–4749.
- [14] G. Shemer, O. Krichevski, G. Markovich, T. Molotsky, I. Lubitz, [A. B. Kotlyar, *J. Am. Chem. Soc.* **2006**, *128*, 11006–11007.
- [15] C. Gautier, T. Bürgi, *ChemPhysChem* **2009**, *10*, 483–492.
- [16] V. Humblot, S. Haq, C. Muryn, W. A. Hofer, R. Raval, *J. Am. Chem. Soc.* **2002**, *124*, 503–510.
- [17] M. Ortega Lorenzo, C. J. Baddeley, C. Muryn, R. Raval, *Nature* **2000**, *404*, 376–379.
- [18] J. A. Fan, C. Wu, K. Bao, J. Bao, R. Bardhan, N. J. Halas, V. N. Manoharan, P. Nordlander, G. Shvets, F. Capasso, *Science* **2012**, *328*, 1135.
- [19] A. Guerrero-Martinez, B. Auguier, J. Lorenzo Alonso-Gomez, Z. Dzolic, S. Gomez-Grana, M. Zinic, M. Magdalena Cid, L. M. Liz-Marzan, *Angew. Chem. Int. Ed.* **2011**, *50*, 5499–5503.
- [20] M. Hentschel, M. Schaferling, T. Weiss, N. Liu, H. Giessen, *Nano Lett.* **2012**, *12*, 2542–2547.
- [21] Z. Fan, A. O. Govorov, *Nano Lett.* **2010**, *10*, 2580–2587.
- [22] A. J. Mastroianni, S. A. Claridge, A. Paul Alivisatos, *J. Am. Chem. Soc.* **2009**, *131*, 8455–8459.
- [23] A. O. Govorov, *J. Phys. Chem. C* **2011**, *115*, 7914–7923.
- [24] A. O. Govorov, Z. Fan, P. Hernandez, J. M. Slocik, R. R. Naik, *Nano Lett.* **2010**, *10*, 1374–1382.
- [25] V. A. Geérard, Y. K. Gun'ko, E. Defranco, A. O. Govorov, *Chem. Commun.* **2011**, *47*, 7383–7385.
- [26] N. A. Abdulrahman, Z. Fan, T. Tonooka, S. M. Kelly, N. Gadegaard, E. Hendry, A. O. Govorov, M. Kadodwala, *Nano Lett.* **2012**, *12*, 977–983.
- [27] D. R. Smith, J. B. Pendry, M. C. K. Wiltshire, *Science* **2004**, *305*, 788.
- [28] C. M. Soukoulis, M. Kafesaki, E. N. Economou, *Adv. Mater.* **2006**, *18*, 1941.
- [29] C. M. Soukoulis, S. Linden, M. Wegener, *Science* **2007**, *315*, 47.
- [30] R. A. Shelby, D. R. Smith, S. Schultz, *Science* **2001**, *292*, 77.
- [31] S. Tretyakov, I. Nefedov, A. Sihvola, S. Maslovski, C. Simovski, *J. Electromagn. Waves. Appl.* **2003**, *17*, 695.
- [32] J. B. Pendry, *Science* **2004**, *306*, 1353.
- [33] C. Monzon, D. W. Forester, *Phys. Rev. Lett.* **2005**, *95*, 123904.
- [34] E. Plum, J. Zhou, J. Dong, V. A. Fedotov, T. Koschny, C. M. Soukoulis, N. I. Zheludev, *Phys. Rev. B* **2009**, *79*, 035407.
- [35] A. V. Rogacheva, V. A. Fedotov, A. S. Schwanecke, N. I. Zheludev, *Phys. Rev. Lett.* **2006**, *97*, 177401.
- [36] J. Zhou, J. Dong, B. Wang, T. Koschny, M. Kafesaki, C. M. Soukoulis, *Phys. Rev. B* **2009**, *79*, 121104(R).
- [37] S. Zhang, Y.-S. Park, J. Li, X. Lu, W. Zhang, X. Zhang, *Phys. Rev. Lett.* **2009**, *102*, 023901.
- [38] E. Plum, V. A. Fedotov, A. S. Schwanecke, N. I. Zheludev, Y. Chen, *Appl. Phys. Lett.* **2007**, *90*, 223113.

- [39] M. Decker, M. W. Klein, M. Wegener, S. Linden, *Opt. Lett.* **2007**, *32*, 856.
- [40] R. Zhao, L. Zhang, J. Zhou, Th. Koschny, C. M. Soukoulis, *Phys. Rev. B* **2011**, *83*, 035105.
- [41] M. Ren, E. Plum, J. Xu, N. I. Zheludev, *Nat. Commun.* **2012**, *3*, 833.
- [42] M. Decker, R. Zhao, C. M. Soukoulis, S. Linden, M. Wegener, *Opt. Lett.* **2010**, *35*, 1593–1595.
- [43] X. Xiong, W.-H. Sun, Y.-J. Bao, M. Wang, R.-W. Peng, C. Sun, X. Lu, J. Shao, Z.-F. Li, N.-B. Ming, *Phys. Rev. B* **2010**, *81*, 075119.
- [44] C. Helgert, E. Pshenay-Severin, M. Falkner, C. Menzel, C. Rockstuhl, E.-B. Kley, A. Tunnermann, F. Lederer, T. Pertsch, *Nano Lett.* **2011**, *11*, 4400–4404.
- [45] B. Wang, J. Zhou, T. Koschny, C. M. Soukoulis, *Appl. Phys. Lett.* **2009**, *94*, 151112.
- [46] J. K. Gansel, M. Thiel, M. S. Rill, M. Decker, K. Bade, V. Saile, G. von Freymann, S. Linden, M. Wegener, *Science* **2009**, *325*, 1513.
- [47] R. Zhao, J. Zhou, Th. Koschny, E. N. Economou, C. M. Soukoulis, *Phys. Rev. Lett.* **2009**, *103*, 103602.
- [48] B. Wang, J. Zhou, Th. Koschny, M. Kafesaki, C. M. Soukoulis, *J. Opt. A: Pure Appl. Opt.* **2009**, *11*, 114003.
- [49] N. Young Ha, Y. Ohtsuka, S. Moon Jeong, S. Nishimura, G. Suzuki, Y. Takanishi, K. Ishikawa, H. Takezoe, *Nat. Mater.* **2008**, *7*, 43–47.
- [50] Y. Tang, A. E. Cohen, *Science* **2011**, *332*, 333.
- [51] N. Yang, A. E. Cohen, *J. Phys. Chem. B* **2012**, dx.doi.org/10.1021/jp1092898.
- [52] Y. Tang, A. E. Cohen, *Phys. Rev. Lett.* **2010**, *104*, 163901.
- [53] I. Hargittai, M. Hargittai, in *Symmetry through the Eyes of a Chemist*, Plenum Press, New York and London, **1995**.
- [54] M. Kuwata-Gonokami, N. Saito, Y. Ino, M. Kauranen, K. Jefimovs, T. Vallius, J. Turunen, Y. Svirko, *Phys. Rev. Lett.* **2005**, *95*, 227401.
- [55] V. K. Valev, B. De Clercq, X. Zheng, D. Denkova, E. J. Osley, S. Vandendriessche, A. V. Silhanek, V. Volskiy, P. A. Warburton, G. A. E. Vandenbosch, M. Ameloot, V. V. Moshchalkov, T. Verbiest, *Opt. Express* **2012**, *20*, 256–264.
- [56] V. K. Valev, N. Smisdov, A. V. Silhanek, B. De Clercq, W. Gillijns, M. Ameloot, V. V. Moshchalkov, T. Verbiest, *Nano Lett.* **2009**, *9*, 3945.
- [57] M. Decker, M. Ruther, C. E. Kriegler, J. Zhou, C. M. Soukoulis, S. Linden, M. Wegener, *Opt. Lett.* **2009**, *34*, 2501.
- [58] M. J. Huttunen, G. Bautista, M. Decker, S. Linden, M. Wegener, M. Kauranen, *Opt. Mat. Express* **2011**, *1*, 46.
- [59] N. Liu, H. Liu, S. Zhu, H. Giessen, *Nat. Phot.* **2009**, *3*, 157.
- [60] M. Decker, R. Zhao, C. M. Soukoulis, S. Linden, M. Wegener, *Opt. Lett.* **2010**, *35*, 1593.
- [61] T. Verbiest, M. Kauranen, Y. Van Rompaey, A. Persoons, *Phys. Rev. Lett.* **1996**, *77*, 1456.
- [62] E. Plum, X.-X. Liu, V. A. Fedotov, Y. Chen, D. P. Tsai, N. I. Zheludev, *Phys. Rev. Lett.* **2009**, *102*, 113902.
- [63] A. Belardini, M. C. Larciprete, M. Centini, E. Fazio, C. Sibilìa, *Phys. Rev. Lett.* **2011**, *107*, 257401.
- [64] C. Noguez, I. L. Garzon, *Chem. Soc. Rev.* **2009**, *38*, 757–771.
- [65] A. Kuzyk, R. Schreiber, Z. Fan, G. Pardatscher, E.-M. Roller, A. Hogege, F. C. Simmel, A. O. Govorov, T. Lied, *Nature* **2012**, *483*, 311.
- [66] A. Radke, T. Gissibl, T. Klotzbücher, P. V. Braun, H. Giessen, *Adv. Mater.* **2011**, *23*, 3018–3021.
- [67] S. Vignolini, N. A. Yufa, P. S. Cunha, S. Guldin, I. Rushkin, M. Stefik, K. Hur, U. Wiesner, J. J. Baumberg, U. Steiner, *Adv. Mater.* **2012**, *24*, OP23–OP27.
- [68] V. K. Valev, X. Zheng, C. G. Biris, A. V. Silhanek, V. Volskiy, B. De Clercq, O. A. Aktsipetrov, M. Ameloot, N. C. Panouiu, G. A. E. Vandenbosch, V. V. Moshchalkov, *Opt. Mater. Express* **2011**, *1*, 36–45.
- [69] M. Stefik, S. Wang, R. Hovden, H. Sai, M. W. Tat, D. A. Muller, U. Steiner, S. M. Gruner, U. Wiesner, *J. Mater. Chem.* **2012**, *22*, 1078–1087.
- [70] C. F. Bohren, *Chem. Phys. Lett.* **1974**, *29*, 458.
- [71] J. David Pendleton, D. L. Rosen, *Appl. Opt.* **1998**, *37*, 7897–7905.
- [72] M. Vrancken, G. A. E. Vandenbosch, *IEEE Trans. Microwave Theory Techn.* **2003**, *51*, 216–225.
- [73] Y. Schols, G. A. E. Vandenbosch, *IEEE Trans. Antennas Propagat.* **2007**, *55*, 1086–1094.
- [74] Lumerical Solutions, inc: <http://www.lumerical.com/>
- [75] A. F. Oskooi, D. Roundy, M. Ibanescu, P. Bermel, J. Joannopoulos, S. G. Johnson, *Comput. Phys. Commun.* **2010**, *181*, 687–702.
- [76] Diffract MOD, RSoft Design Group. <http://www.rsoftdesign.com>
- [77] J. M. Hicks, in *Chirality: Physical Chemistry*, American Chemical Society, Washington, DC, **2002**.
- [78] R. W. Boyd, in *Nonlinear Optics*, Academic Press, San Diego, **1992**.
- [79] C. H. Lee, R. K. Chang, N. Bloembergen, *Phys. Rev. Lett.* **1967**, *18*, 167–170.
- [80] A. Kirilyuk, Th. Rasing, *J. Opt. Soc. Am. B* **2005**, *22*, 148–167.
- [81] Y. Sheng, A. Best, H.-J. Butt, W. Krolikowski, A. Arie, K. Koynov, *Opt. Express* **2010**, *18*, 16539–16545.
- [82] V. V. Pavlov, J. Ferré, P. Meyer, G. Tessier, P. Georges, A. Brun, P. Beauvillain, V. Mathet, *J. Phys. Condens. Matter* **2001**, *13*, 9867–9878.
- [83] V. K. Valev, M. Gruyters, A. Kirilyuk, Th. Rasing, *Phys. Stat. Sol. (b)* **2005**, *242*, 3027–3031.
- [84] Y. R. Shen, in *The Principles of Nonlinear Optics*, John Wiley & Sons, **1984**, p. 6.
- [85] D. L. Mills, in *Nonlinear Optics Basic Concepts*, Springer-Verlag Berlin Heidelberg, **1998**, p. 42.
- [86] S. Foerier, I. A. Kolmychek, O. A. Aktsipetrov, T. Verbiest, V. K. Valev, *ChemPhysChem* **2009**, *10*, 1431.
- [87] M. Kauranen, T. Verbiest, J. J. Maki, A. J. Persoons, *Chem. Phys.* **1994**, *101*, 8193.
- [88] S. Sioncke, T. Verbiest, A. Persoons, *Mater. Sci. Eng., R.* **2003**, *42*, 115.
- [89] V. K. Valev, D. Denkova, X. Zheng, A. I. Kuznetsov, C. Reinhardt, B. N. Chichkov, G. Tsutsumanova, E. J. Osley, V. Petkov, B. De Clercq, A. V. Silhanek, Y. Jeyaram, V. Volskiy, P. A. Warburton, G. A. E. Vandenbosch, S. Russev, O. A. Aktsipetrov, M. Ameloot, V. V. Moshchalkov, T. Verbiest, *Adv. Mater.* **2012**, *24*, OP29–OP35.
- [90] K. J. Savage, M. M. Hawkeye, R. Esteban, A. G. Borisov, J. Aizpurua, J. J. Baumberg, *Nature* **2012**, *491*, 574.
- [91] M. Kuwata-Gonokami, N. Saito, Y. Ino, M. Kauranen, K. Jefimovs, T. Vallius, J. Turunen, Y. Svirko, *Phys. Rev. Lett.* **2005**, *95*, 227401.
- [92] A. V. Zayats, I. I. Smolyaninov, C. C. Davis, *Opt. Commun.* **1999**, *169*, 93–96.
- [93] C. Anceau, S. Brasselet, J. Zyss, P. Gadenne, *Opt. Lett.* **2003**, *28*, 713–715.
- [94] I. Berline, C. Fiorini-Debuisschert, C. Royal, L. Douillard, F. Charra, *J. Appl. Phys.* **2008**, *104*, 103113.
- [95] M. Zavelani-Rossi, M. Celebrano, P. Biagioni, D. Polli, M. Finazzi, L. Duò, G. Cerullo, M. Labardi, M. Allegrini, J. Grand, P.-M. Adam, *Appl. Phys. Lett.* **2008**, *92*, 093119.
- [96] V. K. Valev, A. V. Silhanek, B. De Clercq, W. Gillijns, Y. Jeyaram, X. Zheng, V. Volskiy, O. A. Aktsipetrov, G. A. E. Vandenbosch, M. Ameloot, V. V. Moshchalkov, T. Verbiest, *Small* **2011**, *7*, 2573–2576.
- [97] V. K. Valev, A. Volodin, A. V. Silhanek, W. Gillijns, B. De Clercq, Y. Jeyaram, H. Paddubrouskaya, C. G. Biris, N. C. Panouiu, O. A. Aktsipetrov, M. Ameloot, V. V. Moshchalkov, T. Verbiest, *ACS Nano* **2011**, *5*, 91–96.
- [98] M. Schaferling, D. Dregely, M. Hentschel, H. Giessen, *Phys. Rev. X* **2012**, *2*, 031010.
- [99] T. Nishino, Y. Umezawa, *Anal. Chem.* **2008**, *80*, 6968–6973.
- [100] M. Babiker, C. R. Bennett, D. L. Andrews, L. C. Davila Romero, *Phys. Rev. Lett.* **2002**, *89*, 143601.

- [101] F. Araoka, T. Verbiest, K. Clays, A. Persoons, *Phys. Rev. A* **2005**, 71, 055401.
- [102] K. Toyoda, K. Miyamoto, N. Aoki, R. Morita, T. Omatsu, *Nano Lett.* **2012**, 12, 3645–3649.
- [103] N. M. Litchinitser, *Science* **2012**, 337, 1054.
- [104] V. K. Valev, B. De Clercq, C. G. Biris, X. Zheng, S. Vandendriessche, M. Hojeij, D. Denkova, Y. Jeyaram, N. C. Panoiu, Y. Ekinci, A. V. Silhanek, V. Volskiy, G. A. E. Vandenbosch, M. Ameloot, V. V. Moshchalkov, T. Verbiest, *Adv. Mater.* **2012**, 24, OP208–OP215.
- [105] J. W. Canary, *Chem. Soc. Rev.* **2009**, 38, 747–756.
- [106] B. L. Feringa, *J. Org. Chem.* **2007**, 72, 6635–6652.
- [107] S. Zhang, J. Zhou, Y.-S. Park, J. Rho, R. Singh, S. Nam, A. K. Azad, H.-T. Chen, X. Yin, A. J. Taylor, X. Zhang, *Nat. Commun.* **2012**, 3, 942.
-